Hexakis(pentafluorooxotellurato)pnictate(V) Anions, $M(OTeF_5)_6^-$ (M = As, Sb, Bi): A Series of Very Weakly Coordinating Anions

Hélène P. A. Mercier, Jeremy C. P. Sanders, and Gary J. Schrobilgen*

Contribution from the Department of Chemistry, McMaster University, Hamilton, Ontario L8S 4M1, Canada

*Received June 28, 1993**

Abstract: The weakly coordinating pnicogen anion series, $M(OTeF_5)_6^-$ (M = As, Sb, Bi), has been synthesized as their tetraalkylammonium salts and have been structurally characterized by X-ray crystallography, ^{19}F, ^{75}As, $^{121,123}Sb$, ^{125}Te, ^{209}Bi NMR spectroscopy, and Raman spectroscopy. The following crystal structures are reported: $N(CH_3)_4^+As(OTeF_5)_6^-$, trigonal system, space group $R\bar{3}$, a = 10.109(2) Å, c = 55.443(18) Å, V = 4907 Å^3, D_{calc} = 3.209 g cm^{-3}, Z = 6, R = 0.0644; $N(CH_3)_4^+Sb(OTeF_5)_6^-$, monoclinic system, space group $C2/c$, a = 17.875(3) Å, b = 10.448(2) Å, c = 19.752(2) Å, β = 110.83(1)°, V = 3447.8 Å^3, D_{calc} = 3.135 g cm^{-3}, Z = 4, R = 0.0710; $N(CH_2CH_3)_4^+Sb(OTeF_5)_6^-$, monoclinic system, space group $C2/c$, a = 10.506(3) Å, b = 18.370(6) Å, c = 20.352(7) Å, β = 91.23(2)°, V = 3926.9 Å^3, D_{calc} = 2.848 g cm^{-3}, Z = 4, R = 0.0548; $N(CH_3)_4^+Bi(OTeF_5)_6^-$, triclinic system, space group $P\bar{1}$, a = 8.945(2) Å, b = 9.217(2) Å, c = 10.029(2) Å, α = 100.03(3)°, β = 99.95(3)°, γ = 98.06(3)°, V = 789.5 Å^3, D_{calc} = 3.606 g cm^{-3}, Z = 1, R = 0.0456. The central pnicogen atoms of the anions are bonded octahedrally to the six oxygen atoms and each of the six tellurium atoms is octahedrally bonded to an oxygen and five fluorines. Each anion structure can be described as composed of an octahedron of octahedra. Average M–O bond distances (corrected for libration) and M–O–Te bond angles are As–O = 1.807 Å, Sb–O = 1.96/1.91 Å, Bi–O = 2.065 Å and As–O–Te = 140(2)°, Sb–O–Te = 150.9(8)/162.8(9)°, Bi–O–Te = 136.2(3)°. Low electric field gradients at the pnicogen nuclei result in spin–lattice relaxation times which are sufficiently long to allow for the observation of the NMR spectra of the four quadrupolar pnicogen nuclei and their couplings to ^{125}Te. The anions are nonlabile on the NMR time scale in both SO_2ClF and CH_3CN solvents. Key frequencies in the Raman spectra of the three anions have been assigned. The $M(OTeF_5)_6^-$ anions are likely to be weaker $OTeF_5^-$ donors and less basic than current examples of weakly coordinating anion derivatives of the $OTeF_5$ group, i.e., $B(OTeF_5)_4^-$, $Pd(OTeF_5)_4^{2-}$, $Nb(OTeF_5)_6^-$, and $Ti(OTeF_5)_6^{2-}$.

Introduction

Truly non-coordinating anions (solvents) have eluded those who have been interested in generating coordinatively unsaturated cations. The mythic notion of a truly non-coordinating anion[1] is underscored by the classical "non-coordinating" anions ClO_4^-,[2] $CF_3SO_3^-$,[3] FSO_3^-,[3] BF_4^-,[4] PF_6^-,[5] AsF_6^-,[6] SbF_6^-,[7] BiF_6^-,[8] and BPh_4^-,[9] which are all found to coordinate to metal ions ranging over the Periodic Table and, in many instances, examples of their interaction with non-metal centers are also known. Anions, by definition, interact with electron pair acceptors and it is only a question of degree, so that a semantic down shift to "weakly coordinating anions" is more realistic. The early and continuing use of classical weakly coordinating anions of low nucleophilicity such as BF_4^-, SbF_6^-, $SbCl_6^-$, $Sb_2F_{11}^-$, and those derived from superacid media[10] have proven highly successful in stabilizing Meerwein salts (tertiary carboxonium salts)[11] and main-group cations[12,13] and have been instrumental in the development of the now burgeoning field of stable carbocation chemistry[14–16] and the relatively new field of protosolvated superelectrophiles.[14] More recently, examples of larger and more weakly coordinating anions have been forthcoming that are associated with the quest for the penultimate "least coordinating anion" (ref 17 should be consulted for a comprehensive overview of the subject). Included in this new generation of weakly coordinating anions are $CB_{11}H_{12}^-$ [18–20]

* Abstract published in *Advance ACS Abstracts,* March 1, 1994.

(1) Rosenthal, M. R. *J. Chem. Educ.* **1973**, *50*, 331.

(2) Gowda, N. M. N.; Naiker, S. B.; Reddy, G. K. N. *Adv. Inorg. Chem. Radiochem.* **1984**, *28*, 255.

(3) Lawrence, G. A. *Chem. Rev.* **1986**, *86*, 17.

(4) For example: (a) Cockman, R. W.; Hoskins, B. F.; McCormick, M. J.; O'Donnell, T. A. *Inorg. Chem.* **1988**, *27*, 2742. (b) Horn, E.; Snow, M. R.; Tiekink, E. R. T. *Aust. J. Chem.* **1987**, *40*, 761.

(5) For example: (a) Honeychuck, R. V.; Hersh, W. H. *Inorg. Chem.* **1989**, *28*, 2869. (b) Dartiguenave, M.; Dartiguenave, Y.; Mari, A.; Oliver, M. J.; Beauchamp, A. L. *Can. J. Chem.* **1988**, *66*, 2386.

(6) For example: (a) Faggiani, R.; Gillespie, R. J.; Lock, C. J. L.; Vekris, J. E. *Inorg. Chem.* **1988**, *27*, 4350. (b) Cutforth, B. D.; Gillespie, R. J.; Ireland, P.; Sawyer, J. F.; Ummat, P. K. *Inorg. Chem.* **1983**, *22*, 1344. (c) Zalkin, A.; Ward, D. L.; Biagioni, R. N.; Templeton, D. H.; Bartlett, N. *Inorg. Chem.* **1978**, *17*, 1318. (d) Bartlett, N.; DeBoer, B. G.; Hollander, F. J.; Sladky, F. O.; Templeton, D. H.; Zalkin, A. *Inorg. Chem.* **1973**, *12*, 1717.

(7) For example: (a) Mercier, H. P. A.; Sanders, J. C. P.; Schrobilgen, G. J. *Inorg. Chem.* **1993**, *32*, 386. (b) Boldrini, P.; Gillespie, R. J.; Ireland, P. R.; Schrobilgen, G. J. *Inorg. Chem.* **1974**, *13*, 1690. (c) McKee, D. E.; Zalkin, A.; Bartlett, N. *Inorg. Chem.* **1973**, *12*, 1713. (d) Hersh, W. H. *J. Am. Chem. Soc.* **1985**, *107*, 4599. (e) Shelly, K.; Bartczak, T.; Scheidt, W. R.; Reed, C. A. *Inorg. Chem.* **1985**, *24*, 4325.

(8) Gillespie, R. J.; Martin, D.; Schrobilgen, G. J.; Slim, D. R. *J. Chem. Soc., Dalton Trans.* **1978**, 2234.

(9) For example: (a) Ananias de Carvallio, L. C.; Dartiguenave, M.; Dartiguenave, Y.; Beauchamp, A. L. *J. Chem. Soc.* **1984**, *106*, 6848. (b) Albano, P.; Aresta, M.; Manassero, M. *Inorg. Chem.* **1980**, *19*, 1069.

(10) (a) Olah, G. A.; Prakash, G. K. S.; Sommer, J. *Superacids*; Wiley-Interscience: New York, 1985, and references therein. (b) Gillespie, R. J. *Acc. Chem. Res.* **1968**, *1*, 202.

(11) Perst, H. *Oxonium Ions in Organic Chemistry*; Verlag Chemie: Weinheim, 1971.

(12) Burford, N.; Passmore, J.; Sanders, J. C. P. The Preparation, Structure and Energetics of the Homopolyatomic Cations of Groups 16 and 17. In *Molecular Structure and Energetics*; Liebman, J. F., Greenberg, A., Eds.; Verlag Chemie: New York, 1989; Vol. 11, pp 53–108.

(13) (a) Selig, H.; Holloway, J. H. Cationic and Anionic Complexes of the Noble Gases. In *Topics in Current Chemistry*; Boschke, F. L., Ed.; Springer-Verlag: Berlin, 1984; Vol. 124, pp 33–90. (b) Schrobilgen, G. J. Lewis Acid Properties of Noble Gas Cations. In *Synthetic Fluorine Chemistry*; Chambers, R. D., Olah, G. A., Prakash, G. K. S., Eds.; Wiley and Sons: New York, 1992; Chapter 1, pp 1–30.

(14) Olah, G. A. *Angew. Chem., Int. Ed. Engl.* **1993**, *32*, 767 and references therein.

(15) Olah, G. A. *Angew. Chem., Int. Ed. Engl.* **1973**, *12*, 1763.

(16) Olah, G. A. *Carbocations and Electrophilic Reactions*; Verlag Chemie: Weinheim, 1973/Wiley: New York, 1974 and references therein.

(17) Strauss, S. H. *Chem. Rev.* **1993**, *93*, 927.

(18) Shelly, K.; Reed, C. A.; Lee, Y. J.; Scheidt, W. R. *J. Am. Chem. Soc.* **1986**, *108*, 3117.

0002-7863/94/1516-2921$04.50/0

and related carborane anions such as *closo*-6,7,8,9,10-$Br_5CB_9H_5^-$,[21] heteropolyanions of the Keggin type,[22] a number of fluorinated tetrakisborate anions, e.g., $B(C_6F_5)_4^-$ [23] and $B(3,5\text{-}C_6H_3(CF_3)_2)_4^-$,[24] and several anion derivatives of the highly electronegative $OTeF_5$ group, $B(OTeF_5)_4^-$,[25] $Pd(OTeF_5)_4^{2-}$,[26] $Ti(OTeF_5)_6^{2-}$,[27] $Nb(OTeF_5)_6^-$,[28] and $Ta(OTeF_5)_6^-$.[28]

With their negative charges distributed over 20 and 30 fluorine ligands, the $B(OTeF_5)_4^-$,[29] $Pd(OTeF_5)_4^{2-}$,[26] $Nb(OTeF_5)_6^-$,[30] and $Ti(OTeF_5)_6^{2-}$ [30] anions have shown promise as weakly basic anions and have recently been exploited by Strauss and co-workers as least coordinating anions to produce compounds in which metal ions are coordinately unsaturated and hence highly reactive. While all are stable with respect to fluoride abstraction, delocalization of the negative charge in these anions over a large number of fluorine atoms serves to further diminish their fluoride ion basicities and fluorine–cation interactions. However, the tetrakis anions, $B(OTeF_5)_4^-$ and $Pd(OTeF_5)_4^{2-}$, compete with the solvent for metal coordination sites and show a tendency to form relatively strong M–O···Ag or very weak Te–F···Tl bridges by coordination through their oxygen or fluorine atoms to the metal atom cation centers, cf. $Tl(mes)_2^+B(OTeF_5)_4^-$,[29e] $Tl(1,2\text{-}C_2H_4Cl_2)^+B(OTeF_5)_4^-$,[29b] $Ag(CO)^+B(OTeF_5)_4^-$,[29d] $Ag^+B(OTeF_5)_4^-$,[29c] $[Ag_2(CH_2Cl_2)_4]^{2+}Pd(OTeF_5)_4^{2-}$,[26] and $[Ag_2(1,2\text{-}C_2H_4Cl_2)_4]^{2+}Pd(OTeF_5)_4^{2-}$.[26] Recent studies of the lability of $OTeF_5$ groups in $Nb(OTeF_5)_6^-$ and $B(OTeF_5)_4^-$ show that the sterically more hindered $Nb(OTeF_5)_6^-$ anion is kinetically more stable.[30] The effect of a sterically more hindered octahedral anion is also apparent in $[Ag(CH_2Cl_2)_3]_2^{2+}Ti(OTeF_5)_6^{2-}$ where the less accessible oxygen cannot bridge to the metal and all metal coordination sites are occupied by the solvent and weak metal–anion interactions consisting of Ag···F–Te bridges.[30]

From a consideration of the properties of known anions consisting of fully substituted $OTeF_5$ groups, it is possible to propose a set of criteria for even less coordinating anions of this genre: (1) the neutral parent must have a higher $OTeF_5^-$ affinity (i.e., must be a stronger $OTeF_5^-$ acceptor) than previously known Lewis acid precursors, e.g., $B(OTeF_5)_3$ and $Nb(OTeF_5)_5$, to prevent $OTeF_5^-$ transfer to the cationic site, (2) the resulting anion must be even less basic than $B(OTeF_5)_4^-$, $Pd(OTeF_5)_4^{2-}$, $Nb(OTeF_5)_6^-$, and $Ti(OTeF_5)_6^{2-}$ and should be univalent with the negative charge spread over as many fluorine ligands as possible, (3) the oxygen base sites should be sterically inaccessible to the cation and for this reason octahedral anions are preferred, and (4) the anion must be resistant to oxidative attack by electrophilic cations.

Likely candidates for even more weakly coordinating anions are the $OTeF_5$ derivatives of the powerful fluoro-acids and Lewis acids AsF_5, SbF_5, and BiF_5 whose pentakis(pentafluorooxotellurate) derivatives should be stronger $OTeF_5$ acceptors than either $Nb(OTeF_5)_5$ or $Ti(OTeF_5)_5^-$, and it is anticipated that $HOTeF_5$ should function as a strong acid in the presence of $M(OTeF_5)_5$ (M = As, Sb, Bi). The large $M(OTeF_5)_6^-$ anions appear to meet all the criteria mentioned above and can be anticipated to be useful in stabilizing novel inorganic main-group and coordinatively unsaturated metal cations by virtue of their abilities to disperse a single negative charge over 30 fluorines and to provide sterically less accessible oxygen base centers. However, the low nucleophilicities of the hexafluoro-anion analogs and of their related polymeric anions, e.g., $Sb_2F_{11}^-$, $Bi_2F_{11}^-$, $Sb_3F_{16}^-$, are well-established[10-16] and difficult to rival. The relative degree of $M(OTeF_5)_6^-$ anion nucleophilicity will, in large measure, be determined by steric accessibility of the oxygen electron lone pairs, which can be anticipated to be less available in octahedral $M(OTeF_5)_6^-$ anions than in tetrahedral $B(OTeF_5)_4^-$.

We have previously prepared $As(OTeF_5)_5$ and shown that it functions as a strong $OTeF_5$ acceptor by analogy with AsF_5 and AsF_6^- to form the $As(OTeF_5)_6^-$ anion, which we have characterized in solution by ^{19}F and ^{75}As NMR spectroscopy.[31,32] Prior to this work, $As(OTeF_5)_6^-$ was the only group 15 $M(OTeF_5)_6^-$ anion to have been characterized; however, no solid-state characterization of this anion or its antimony and bismuth analogs had been reported. In related work, we have synthesized the first fully $OTeF_5$ substituted salt, $XeOTeF_5^+Sb(OTeF_5)_6^-$, and have investigated the Lewis acid properties of the $XeOTeF_5^+$ cation toward nitrogen bases in SO_2ClF at low temperatures.[33]

The present work reports synthetic approaches which lead to pure $Bi(OTeF_5)_5$ and pure tetraalkylammonium salts of all three pnicogen anions as well as their characterization in solution by ^{19}F, ^{75}As, ^{125}Te, $^{121,123}Sb$, and ^{209}Bi NMR spectroscopy and in the solid state by X-ray crystallography and Raman spectroscopy.

Results and Discussion

Synthesis of $Bi(OTeF_5)_5$ and the $M(OTeF_5)_6^-$ Anions (M = As, Sb, or Bi). (a) $Bi(OTeF_5)_5$. The $OTeF_5$ analog of AsF_5, namely $As(OTeF_5)_5$, has been known for some time and can readily be prepared in good yield from the reaction of $B(OTeF_5)_3$ with AsF_5 in SO_2 solvent.[31,32] All attempts to prepare pure $Sb(OTeF_5)_5$ have been unsuccessful and indicate that this compound is unstable above 0 °C.[32,34] In the present work, the synthesis of hitherto unknown $Bi(OTeF_5)_5$ has been achieved by a route analogous to that used for the preparation of $As(OTeF_5)_5$ (eq 1).

$$3BiF_5 + 5B(OTeF_5)_3 \xrightarrow{\text{Freon-114, 0 °C}} 3Bi(OTeF_5)_5 + 5BF_3 \quad (1)$$

The reaction proceeds at 0 °C to yield $Bi(OTeF_5)_5$ as a yellow powder which is only poorly soluble in Freon-114 ($CClF_2CClF_2$).

(19) (a) Liston, D. J.; Reed, C. A.; Eigenbrot, C. W.; Scheidt, W. R. *Inorg. Chem.* **1987**, *26*, 2760. (b) Shelly, K.; Finister, D. C.; Lee, Y. J.; Scheidt, W. R.; Reed, C. A. *J. Am. Chem. Soc.* **1985**, *107*, 5955.

(20) (a) Liston, D. J.; Lee, Y. J.; Scheidt, W. R.; Reed, C. A. *J. Am. Chem. Soc.* **1989**, *111*, 6643. (b) Gupta, G. P.; Lang, G.; Young, J. Y.; Scheidt, W. R.; Reed, C. A. *Inorg. Chem.* **1987**, *26*, 3022.

(21) (a) Xie, Z.; Liston, D. J.; Jelínek, T.; Mitro, V.; Bau, R.; Reed, C. A. *J. Chem. Soc., Chem. Commun.* **1993**, 384. (b) Jelínek, T.; Baldwin, P.; Scheidt, W. R.; Reed, C. A. *Inorg. Chem.* **1993**, *32*, 1982.

(22) (a) Siedle, A. R.; Gleason, W. B.; Newmark, R. A.; Skarjune, R. P.; Lyon, P. A.; Markell, C. G.; Hodgson, K. O.; Roe, A. L. *Inorg. Chem.* **1990**, *29*, 1667. (b) Siedle, A. R.; Newmark, R. A.; Sahyum, M. R. V.; Lyon, P. A.; Hunt, S. L.; Skarjune, R. P. *J. Am. Chem. Soc.* **1989**, *111*, 8346. (c) Siedle, A. R.; Newmark, R. A. *J. Am. Chem. Soc.* **1989**, *111*, 2058. (d) Siedle, A. R.; Newmark, R. A. *Organometallics* **1989**, *8*, 1442. (e) Siedle, A. R. *New J. Chem.* **1989**, *13*, 719. (f) Siedle, A. R.; Newmark, R. A.; Gleason, W. B.; Skarjune, R. P.; Hodgson, K. O.; Roe, A. L.; Day, V. W. *Solid State Ionics* **1988**, *26*, 109. (g) Siedle, A. R.; Newmark, R. A.; Brown-Wensley, K. A.; Skarjune, R. P.; Haddad, L. C.; Hodgson, K. O.; Roe, A. L. *Organometallics* **1988**, *7*, 2078. (h) Siedle, A. R.; Markell, C. G.; Lyon, P. A.; Hodgson, K. O.; Roe, A. L. *Inorg. Chem.* **1987**, *26*, 219.

(23) (a) Lambert, J. B.; Zhang, S. *J. Chem. Soc., Chem. Commun.* **1993**, 383. (b) Marks, T. J. *Acc. Chem. Res.* **1992**, *25*, 57. (c) Yang, X.; Stern, C. L.; Marks, T. J. *Organometallics* **1991**, *10*, 840. (d) Chlen, J. C. W.; Tsai, W-M.; Rausch, M. D. *J. Am. Chem. Soc.* **1991**, *113*, 8570.

(24) (a) Nishida, H.; Takada, N.; Yoshimura, M.; Sonoda, T.; Kobayashi, H. *Bull. Chem. Soc. Jpn.* **1984**, *57*, 2600. (b) Brookhart, M.; Rix, R. C.; DeSimone, J. M.; Barborak, J. C. *J. Am. Chem. Soc.* **1992**, *114*, 5894. (c) Taube, R.; Wache, S. *J. Organomet. Chem.* **1992**, *428*, 431. (d) Horton, A. D.; Orpen, A. G. *Organometallics* **1991**, *10*, 3910. (e) Brookhart, M.; Sabo-Etienne, S. *J. Am. Chem. Soc.* **1991**, *113*, 2778.

(25) Kropshofer, H.; Leitzke, O.; Peringer, P.; Sladky, F. *Chem. Ber.* **1981**, *114*, 2644.

(26) Colsman, M. R.; Newbound, T. D.; Marshall, L. J.; Noirot, M. D.; Miller, M. M.; Wulfsberg, G. P.; Frye, J. S.; Anderson, O. P.; Strauss, S. H. *J. Am. Chem. Soc.* **1990**, *112*, 2349.

(27) Schröder, K.; Sladky, F. *Chem. Ber.* **1980**, *113*, 1414.

(28) Moock, K.; Seppelt, K. *Z. Anorg. Allg. Chem.* **1988**, *561*, 132.

(29) (a) Hurlburt, P. K.; Rack, J. J.; Dec, S. F.; Anderson, O. P.; Strauss, S. H. *Inorg. Chem.* **1993**, *32*, 373. (b) Hurlburt, P. K.; Anderson, O. P.; Strauss, S. H. *Can. J. Chem.* **1992**, *70*, 726. (c) Van Seggen, D. M.; Hurlburt, P. K.; Anderson, O. P.; Strauss, S. H. *Inorg. Chem.* **1992**, *31*, 1423. (d) Hurlburt, P. K.; Anderson, O. P.; Strauss, S. H. *J. Am. Chem. Soc.* **1991**, *113*, 6277. (e) Noirot, M. D.; Anderson, O. P.; Strauss, S. H. *Inorg. Chem.* **1987**, *26*, 2216.

(30) Van Seggen, D. M.; Hurlburt, P. K.; Anderson, O. P.; Strauss, S. H. *J. Am. Chem. Soc.* **1992**, *114*, 10995.

(31) Collins, M. J.; Rao, U. R. K.; Schrobilgen, G. J. *J. Magn. Reson.* **1985**, *61*, 137.

(32) Collins, M. J.; Schrobilgen, G. J. *Inorg. Chem.* **1985**, *24*, 2608.

(33) Sanders, J. C. P.; Schrobilgen, G. J., to be submitted for publication.

(34) Lentz, D.; Seppelt, K. *Z. Anorg. Allg. Chem.* **1983**, *502*, 83.

The compound is stable at room temperature but is extremely moisture sensitive and rapidly turns reddish-brown on exposure to moist air.

The ^{19}F NMR spectrum of $Bi(OTeF_5)_5$ in Freon-114 at −10 °C displays a single AB_4 pattern with the chemical shifts of the A and B_4 parts well separated [δ(A), −47.5 ppm; δ(B), −35.8 ppm; $^2J(^{19}F_A-^{19}F_B)$, 180 Hz; $^1J(^{19}F_A-^{125}Te)$, 3648 Hz; $^1J(^{19}F_B-^{125}Te)$, 3691 Hz]. The observation of only one AB_4 pattern, rather than the two expected for a trigonal-bipyramidal structure, demonstrates that all the $OTeF_5$ ligands have been rendered equivalent and that, like $As(OTeF_5)_5$,[32] $Bi(OTeF_5)_5$ is fluxional. Attempts to slow down the exchange by cooling the sample were unsuccessful owing to the poor solubility of $Bi(OTeF_5)_5$ at temperatures lower than −10 °C.

(b) $M(OTeF_5)_6^-$ Anions (M = As, Sb, or Bi). The $N(CH_3)_4^+$ salts of the $As(OTeF_5)_6^-$ and $Bi(OTeF_5)_6^-$ anions have been prepared by the reaction of the appropriate $M(OTeF_5)_5$ derivative (M = As or Bi) with a small excess of $N(CH_3)_4^+OTeF_5^-$ in SO_2ClF according to eq 2.

$$M(OTeF_5)_5 + N(CH_3)_4^+OTeF_5^- \xrightarrow{SO_2ClF,\ 25\ °C} N(CH_3)_4^+M(OTeF_5)_6^- \quad (2)$$

(M = As or Bi)

The instability of $Sb(OTeF_5)_5$[35] makes it inconvenient to use this compound for the synthesis of $Sb(OTeF_5)_6^-$ salts and thus a different route has been employed. This involves a two-step process in which the $Sb(OTeF_5)_4^-$ anion is first formed as an intermediate and then oxidized to $Sb(OTeF_5)_6^-$ with $Xe(OTeF_5)_2$ according to eqs 3 and 4.

$$NR_4^+OTeF_5^- + Sb(OTeF_5)_3 \xrightarrow{SO_2ClF,\ 25\ °C} NR_4^+Sb(OTeF_5)_4^- \quad (3)$$

$$NR_4^+Sb(OTeF_5)_4^- + Xe(OTeF_5)_2 \xrightarrow{SO_2ClF,\ 0\ °C} NR_4^+Sb(OTeF_5)_6^- + Xe \quad (4)$$

R = CH_3 or CH_2CH_3

The ability of $Xe(OTeF_5)_2$ to introduce two $OTeF_5$ groups oxidatively has previously been exploited in the synthesis of neutral high-oxidation-state $OTeF_5$ derivatives from the appropriate neutral low-oxidation-state derivatives, e.g., $Te(OTeF_5)_6$ from $Te(OTeF_5)_4$[36] and $I(OTeF_5)_5$ from $I(OTeF_5)_3$.[37] The above preparation of $Sb(OTeF_5)_6^-$ salts represents the first application of this method to the synthesis of fully $OTeF_5$ substituted anionic species.

At 25 °C, the $N(CH_3)_4^+As(OTeF_5)_6^-$, $N(CH_3)_4^+Sb(OTeF_5)_6^-$, $N(CH_3)_4^+Bi(OTeF_5)_6^-$, and $N(CH_2CH_3)_4^+Sb(OTeF_5)_6^-$ salts are readily soluble in the weakly coordinating solvent SO_2ClF and can be isolated as pure crystalline solids by allowing Freon-114, in which the salts are insoluble, to diffuse slowly into the SO_2ClF solutions. All four compounds are stable solids at room temperature. The colors of the salts are interesting: the $Bi(OTeF_5)_6^-$ salt is yellow, while the $As(OTeF_5)_6^-$ and $Sb(OTeF_5)_6^-$ salts are colorless. Similarly, the salt $Li^+Bi(C_6H_5)_6^-$ is reported to be yellow,[38] whereas $Li^+Sb(C_6H_5)_6^-$ is colorless.[39] In addition, neutral $Bi(OTeF_5)_5$ is also yellow. This yellow color appears to be a unique property of the Bi(V) species and may be a consequence of relativistic effects on the heavy Bi atom. In the octahedral anions, relativistic stabilization of the a_{1g} LUMO could result in the first allowed optical transition ($t_{1u} \rightarrow a_{1g}$) moving to a longer wavelength with a tail into the visible spectrum.[40] Pyykkö[40] has shown by quasirelativistic multiple scattering $X\alpha$ calculations that the yellow color of $PbCl_6^{2-}$ is attributable to this effect; contrastingly the lighter congeneric $SnCl_6^{2-}$ anion, in which the relativistic stabilization of the a_{1g} LUMO is less pronounced, is colorless.

The high solubilities of the $NR_4^+M(OTeF_5)_6^-$ salts in the very weakly coordinating solvent SO_2ClF provide a clear indication of the diffuseness of the negative charge in the $M(OTeF_5)_6^-$ anions and of their weakly coordinating nature. The $As(OTeF_5)_6^-$ and $Sb(OTeF_5)_6^-$ salts are also readily soluble, and form stable solutions, in CH_3CN and CH_2Cl_2. However, $N(CH_3)_4^+Bi(OTeF_5)_6^-$ decomposes very slowly in SO_2ClF but quite rapidly in CH_3CN at room temperature. This decomposition is discussed in more detail in the NMR spectroscopy section.

NMR Spectroscopy of $M(OTeF_5)_6^-$ Anions (M = As, Sb, or Bi). (a) ^{75}As, $^{121,123}Sb$, and ^{209}Bi NMR Spectra. The quadrupolar nature of the ^{75}As ($I = 3/2$), ^{121}Sb ($I = 5/2$), ^{123}Sb (I, $7/2$), and ^{209}Bi ($I = 9/2$) nuclides has resulted in their being little exploited for chemical studies, since the highly efficient quadrupolar mechanism which dominates their relaxation behavior tends to produce extremely broad resonances.[41-44] Nevertheless, the few NMR studies in which the ^{75}As,[31,32,45-48] ^{121}Sb,[46,48-52] ^{123}Sb,[48,52,53] and ^{209}Bi[54] nuclides have been employed have clearly demonstrated the usefulness of these nuclides, under certain circumstances, for chemical characterization in solution. The relaxation of a quadrupolar nucleus, under the conditions of extreme narrowing, is described by eq 5

$$\Delta\nu_{1/2} = \frac{1}{\pi T_2} = \frac{1}{\pi T_1} = \frac{3\pi}{10}\left(\frac{2I+3}{I^2(2I-1)}\right)\left(\frac{e^2qQ}{h}\right)^2\left(1+\frac{\eta^2}{3}\right)\tau_c \quad (5)$$

where $\Delta\nu_{1/2}$ is the line width at half-height; T_2 is the spin–spin relaxation time; T_1 is the spin–lattice relaxation time; I is the nuclear spin quantum number; e is the charge on the electron; Q is the nuclear quadrupole moment; eq is the electric field gradient (EFG) along the principle z axis; η is the asymmetry parameter for the EFG; and τ_c is the rotational correlation time.[55] Closer inspection of several of the factors in this equation reveals that line widths are dramatically reduced for nuclides having a high value of I or a small value of Q or both.[56] The merits of the ^{75}As, ^{121}Sb, ^{123}Sb, and ^{209}Bi with regard to these requirements have

(35) Sanders, J. C. P.; Schrobilgen, G. J., unpublished results.
(36) Lentz, D.; Pritzkow, H.; Seppelt, K. *Inorg. Chem.* **1978**, *17*, 1926.
(37) Lentz, D.; Seppelt, K. *Z. Anorg. Allg. Chem.* **1980**, *460*, 5.
(38) Hellwinkel, D.; Kilthau, G. *Liebigs Ann. Chem.* **1967**, *705*, 66.
(39) Wittig, G.; Clauss, K. *Liebigs Ann. Chem.* **1952**, *577*, 26.
(40) El-Issa, B. D.; Pyykkö, P.; Zanati, H. M. *Inorg. Chem.* **1991**, *30*, 2781.
(41) Dixon, K. R. In *Multinuclear NMR*; Mason, J., Ed.; Plenum Press: New York, 1987; Chapter 13, p 369.
(42) Drakenberg, T. In *Annual Reports on NMR Spectroscopy*; Webb, G. A., Ed.; Academic Press: London, 1986; Vol. 17, p 231.
(43) Kidd, R. G. In *The Multinuclear Approach to NMR Spectroscopy*; Lambert, J. B., Riddell, F. G., Eds.; NATO ASI Series C; D. Reidel: Boston, MA, 1983; p 379.
(44) Harris, R. K. In *NMR and the Periodic Table*; Harris, R. K., Mann, B. E., Eds.; Academic Press: London, 1978; Chapter 11, p 379.
(45) Balimann, G.; Pregosin, P. S. *J. Magn. Reson.* **1977**, *26*, 283.
(46) Dove, M. F. A.; Sanders, J. C. P.; Lloyd Jones, E. M.; Parkin, M. J. *J. Chem. Soc., Chem. Commun.* **1984**, 1578.
(47) McGarvey, G. B.; Moffat, J. B. *J. Magn. Reson.* **1990**, *88*, 305.
(48) Sanders, J. C. P. Ph.D. Thesis, University of Nottingham, 1986.
(49) Kidd, R. G.; Matthews, R. W. *J. Inorg. Nucl. Chem.* **1975**, *37*, 661.
(50) Kidd, R. G.; Spinney, H. G. *Can. J. Chem.* **1981**, *59*, 2940.
(51) Goetz-Grandmont, G. J.; Leroy, M. J. F. *Z. Anorg. Allg. Chem.* **1983**, *496*, 40.
(52) Dove, M. F. A.; Sanders, J. C. P. *J. Chem. Soc., Dalton Trans.* **1992**, 3311.
(53) (a) Hatton, J. V.; Saito, Y.; Schneider, W. G. *Can. J. Chem.* **1965**, *43*, 47. (b) Dharmatti, S. S.; Weaver, H. E. *Phys. Rev.* **1952**, *87*, 675. (c) Proctor, W. G.; Yu, F. C. *Phys. Rev.* **1951**, *81*, 20. Cohen, V. W.; Knight, W. D.; Wentink, T. *Phys. Rev.* **1950**, *79*, 191.
(54) Morgan, K.; Sayer, B. G.; Schrobilgen, G. J. *J. Magn. Reson.* **1983**, *52*, 139.
(55) Abragam, A. *The Principles of Nuclear Magnetism*; Oxford University Press; London, 1978; Chapter 8.
(56) Sanders, J. C. P.; Schrobilgen, G. J. In *Multinuclear Magnetic Resonance in Liquids and Solids—Chemical Applications*; Granger, P., Harris, R. K., Eds.; NATO ASI Series C; Kluwer Academic Publishers: Boston, 1990; p 157.

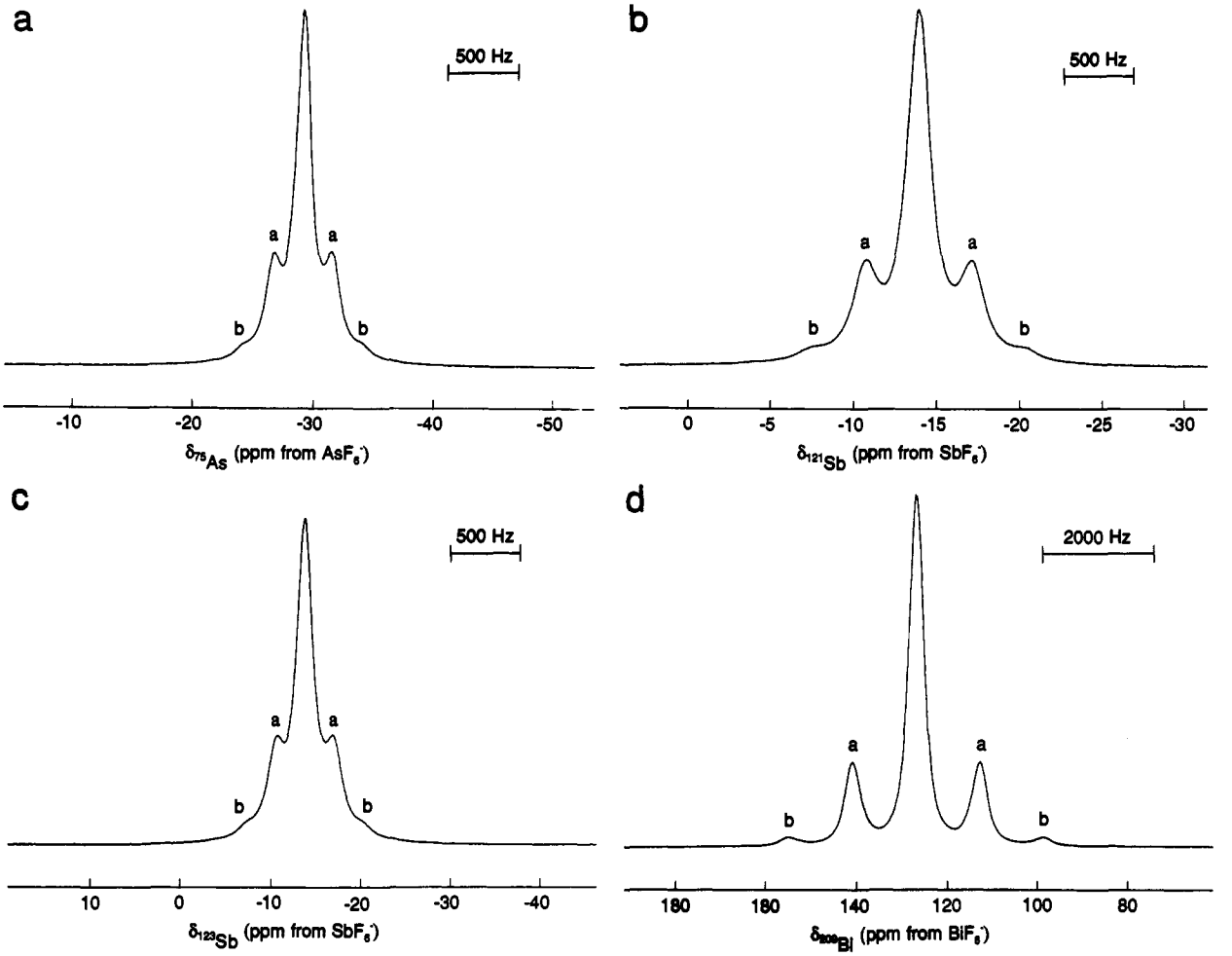

Figure 1. Pnicogen NMR spectra of the $M(OTeF_5)_6^-$ anions (M = As, Sb, or Bi) in CH_3CN at 30 °C: (a) ^{75}As NMR spectrum (85.637 MHz) of $N(CH_3)_4^+As(OTeF_5)_6^-$ (0.05 M); (b) ^{121}Sb NMR spectrum (119.696 MHz) of $N(CH_3)_4^+Sb(OTeF_5)_6^-$ (0.08 M); (c) ^{123}Sb NMR spectrum (64.819 MHz) of $N(CH_3)_4^+Sb(OTeF_5)_6^-$ (0.08 M); (d) ^{209}Bi NMR spectrum (80.637 MHz) of $N(CH_3)_4^+Bi(OTeF_5)_6^-$ (0.06 M). In each spectrum, the ^{125}Te satellites arising from the isotopomers $M(OTeF_5)_5(O^{125}TeF_5)^-$ and $M(OTeF_5)_4(O^{125}TeF_5)_2^-$ are denoted by the labels a and b, respectively.

been discussed previously.[31,32,41-44,48,52,54] Moreover, narrow line widths are known to arise from quadrupolar nuclei residing at the center of a highly symmetric ligand environment (e.g., O_h or T_d) for which the values of q and η are low.[57] The local octahedral environment of the pnicogen nuclei in $As(OTeF_5)_6^-$, $Sb(OTeF_5)_6^-$, and $Bi(OTeF_5)_6^-$ anions affords a low EFG at these nuclei and has allowed definitive characterization of these species in solution by ^{75}As, ^{121}Sb, ^{123}Sb, and ^{209}Bi NMR spectroscopy.

The ^{75}As NMR spectrum of $Cs^+[As(OTeF_5)_6^-]$ in CH_3CN solution has been reported previously together with a line shape analysis which allowed the extraction of the partially resolved two-bond ^{75}As–^{125}Te coupling constant.[31,32] Comparison of these results with those of the present study will be given below.

The NMR spectra for the central pnicogen nuclides in the $As(OTeF_5)_6^-$, $Sb(OTeF_5)_6^-$, and $Bi(OTeF_5)_6^-$ anions are shown in Figure 1. In each case, the spectrum was obtained from a solution of the $N(CH_3)_4^+$ salt in CH_3CN. The ^{75}As NMR spectrum of $N(CH_3)_4^+As(OTeF_5)_6^-$ in CH_3CN is clearly much better resolved than in the previous study and the possible reasons for this will be discussed later in this section. All four spectra display the same basic pattern: a central line flanked by satellites arising from the resolved two-bond coupling between the pnicogen nucleus and ^{125}Te in the isotopomers containing natural abundance (6.99%) ^{125}Te. The individual abundances of the possible ^{125}Te isotopomers for the $M(OTeF_5)_6^-$ anions are given in Table 1. It can be seen that only the first three isotopomers are of sufficient abundance to contribute significantly to the observed spectrum.

Table 1. Statistical Distribution of ^{125}Te Isotopomers in the $M(OTeF_5)_6^-$ Anions (M = As, Sb, or Bi)

isotopomer	% abundance[a]	M multiplet[b]
$M(OTeF_5)_6^-$	64.7	singlet
$M(OTeF_5)_5(O^{125}TeF_5)^-$	29.2	doublet
$M(OTeF_5)_4(O^{125}TeF_5)_2^-$	5.5	triplet
$M(OTeF_5)_3(O^{125}TeF_5)_3^-$	0.5	quartet
$M(OTeF_5)_2(O^{125}TeF_5)_4^-$	0.03	quintet
$M(OTeF_5)(O^{125}TeF_5)_5^-$	9×10^{-4}	sextet
$M(O^{125}TeF_5)_6^-$	1×10^{-5}	septet

[a] Isotopomers containing ^{123}Te ($I = {}^1/_2$; natural abundance 0.87%) were not considered to be of significance and are not included. [b] Binomial multiplets arising from coupling to ^{125}Te ($I = {}^1/_2$; natural abundance 6.99%).

Thus, a singlet will be observed for the most abundant isotopomer, $M(OTeF_5)_6^-$, which contains no magnetically active Te; the next most abundant isotopomer, $M(OTeF_5)_5(O^{125}TeF_5)^-$, will give rise to a 1:1 doublet whose components will each have an intensity which is 21.6% of that for the central singlet; and the last isotopomer of significant abundance, $M(OTeF_5)_4(O^{125}TeF_5)_2^-$, will give rise to a 1:2:1 triplet whose central component will lie under the central singlet arising from the $M(OTeF_5)_6^-$ isotopomer and will contribute 2.75% to the latter's total intensity, while the two outer components (with an intensity 2.0% of the total intensity of the central singlet) will be observed at a spacing of $^2J(M-^{125}Te)$ either side of the central singlet. In the ^{75}As, ^{121}Sb, and ^{123}Sb spectra these components can be seen as shoulders at the base of the main resonance, while in the ^{209}Bi spectrum they are well resolved (Figure 1).

The chemical shift and coupling constant data for the ^{75}As,

(57) Akitt, J. W.; McDonald, W. S. *J. Magn. Reson.* **1984**, *58*, 401. Akitt, J. W. *Prog. NMR Spectrosc.* **1989**, *21*, 401.
(58) Raynes, W. T. *Magn. Reson. Chem.* **1992**, *30*, 686.

Table 2. NMR Parameters for the $M(OTeF_5)_6^-$ Anions (M = As, Sb, or Bi)

$M(OTeF_5)_6^-$	$\delta(M)$,[a,b] ppm	$\delta(^{125}Te)$,[c,d] ppm	$^2J(M-^{125}Te)$, Hz	$^2K(M-Te)$,[e] 10^{21} T^2 J^{-1}	$^2K(M-Te)_{RC}$,[e] 10^{21} T^2 J^{-1}
$^{75}As(OTeF_5)_6^-$	-29.1	534.3	430	6.551	3.954
$^{121}Sb(OTeF_5)_6^-$	-13.9	547.2	785	8.529	4.094
$^{123}Sb(OTeF_5)_6^-$	-13.8	547.2	425	8.526	4.093
$^{209}Bi(OTeF_5)_6^-$	126.7		2269	36.31	7.483

[a] Data obtained from solutions of $N(CH_3)_4^+As(OTeF_5)_6^-$ (0.05 M), $N(CH_3)_4^+Sb(OTeF_5)_6^-$ (0.08 M), and $N(CH_3)_4^+Bi(OTeF_5)_6^-$ (0.06 M) in CH_3CN at 30 °C. [b] Relative to the appropriate MF_6^- reference standard at 30 °C. [c] Data obtained from solutions of $N(CH_3)_4^+As(OTeF_5)_6^-$ (0.08 M) and $N(CH_3)_4^+Sb(OTeF_5)_6^-$ (0.08 M) in CH_3CN at 65 °C. [d] Relative to neat $Te(CH_3)_2$ at 30 °C. [e] In accordance with a recent recommendation, the units T^2 J^{-1} have been employed for the reduced coupling constants instead of the previously used equivalent units N A^{-2} m^{-3}.[58]

^{121}Sb, ^{123}Sb, and ^{209}Bi NMR spectra are summarized in Table 2. The value of the ^{75}As chemical shift is in good agreement with that published in the earlier study for $Cs^+[As(OTeF_5)_6^-]$ in CH_3CN solution and reveals that there is no significant cation dependence on the ^{75}As chemical shift.[31,32] The ^{75}As and $^{121,123}Sb$ chemical shifts of the $As(OTeF_5)_6^-$ and $Sb(OTeF_5)_6^-$ anions occur to low frequency of the respective MF_6^- (M = As or Sb) reference standards, although contrary to expectation $Sb(OTeF_5)_6^-$ is less shielded with respect to SbF_6^- than $As(OTeF_5)_6^-$ is with respect to AsF_6^-. This rather anomalous decrease in shielding sensitivity for the antimony nuclides has been noted previously for $SbCl_6^-$, where an unexpectedly small shielding effect, as compared with those in the analogous PCl_6^- and $AsCl_6^-$ anions,[48,52] is also observed, although the reasons for it are not understood. The greater shielding observed for the $As(OTeF_5)_6^-$ and $Sb(OTeF_5)_6^-$ anions is in accord with the increased shielding anticipated for the less electronegative $OTeF_5$ ligand.[59] In contrast, the ^{209}Bi resonance of the $Bi(OTeF_5)_6^-$ anion, which is only the third ^{209}Bi resonance to be reported,[54] occurs to high frequency of the BiF_6^- reference standard. The reason for this apparently anomalous behavior is unclear at present, but it may be a consequence of the significant relativistic effects on the Bi atom.

The coupling constants $^2J(M-^{125}Te)$ observed for the $M(OTeF_5)_6^-$ anions are presented in Table 2 and are the only known two-bond couplings for the ^{75}As, $^{121,123}Sb$, and ^{209}Bi nuclides. The values of $^2J(^{75}As-^{125}Te)$ and $^2J(^{121,123}Sb-^{125}Te)$ were taken from resolution enhanced ^{75}As, ^{121}Sb, and ^{123}Sb spectra, respectively, in order to obtain values unaffected by overlap of the satellites with the intense central resonance. This procedure was unnecessary in the case of $^2J(^{209}Bi-^{125}Te)$ since the ^{125}Te satellites are well separated from the central resonance in the ^{209}Bi spectrum.

The value of $^2J(^{75}As-^{125}Te)$ obtained for $N(CH_3)_4^+As(OTeF_5)_6^-$ in CH_3CN by direct measurement is in excellent agreement with that obtained previously by line shape analysis of the ^{75}As NMR spectrum of $Cs^+[As(OTeF_5)_6^-]$ in CH_3CN solution (i.e., 430 ± 40 Hz).[31,32] In the $Sb(OTeF_5)_6^-$ anion the value of the ratio $^2J(^{121}Sb-^{125}Te)/^2J(^{123}Sb-^{125}Te)$ is 1.847, which is in excellent accord with the ratio of the magnetogyric ratios of the two antimony nuclides, i.e., $\gamma(^{121}Sb)/\gamma(^{123}Sb) = 1.8467$.

In general, spin–spin coupling between heavy nuclei is dominated by the Fermi contact mechanism when the atoms containing these nuclei are connected by single rather than multiple bonds.[60] In terms of the formalism developed by Pople and Santry,[61] the Fermi contact mechanism is given by the expressions in eqs 6 and 7

$$J(AB) = \frac{16\pi^2}{9h}\left(\frac{g\beta h}{2\pi}\right)^2 \gamma_A\gamma_B|\psi_{ns,A}(0)|^2|\psi_{ns,B}(0)|^2\,\Pi_{AB} \quad (6)$$

$$\Pi_{AB} = 4\sum_{i}^{occ}\sum_{j}^{unocc}\frac{C_{is,A}C_{is,B}C_{js,A}C_{js,B}}{E_j - E_i} \quad (7)$$

where all the symbols have their usual meanings, $|\psi_{ns,A}(0)|^2$ and $|\psi_{ns,B}(0)|^2$ are the s-electron densities for the valence ns orbitals at nuclei A and B, Π_{AB} is the mutual polarizability of the ns orbitals on A and B, $C_{n,A}$ and $C_{n,B}$ are the LCAO coefficients of the s-type atomic orbitals centered on A and B, and E_j and E_i are the energies of the occupied and unoccupied molecular orbitals, respectively. From eq 6 it can be seen that the coupling constant is dependent on the nuclear properties of the coupled nuclei (i.e., the magnetogyric ratios γ_A and γ_B), as well as on the electronic terms (i.e., s-electron density and Π_{AB}).

In order to make comparisons between couplings in a series of related species, it is first necessary to factor out the nuclear dependence and this is accomplished by using the reduced coupling constant, $K(AB)$, defined in eq (8).[61]

$$K(AB) = \frac{4\pi^2 J(AB)}{h\gamma_A\gamma_B} \quad (8)$$

The reduced coupling constants for the $M(OTeF_5)_6^-$ anions are given in Table 2. For a series of structurally related species such as the octahedral $M(OTeF_5)_6^-$ anions, the $K(AB)$ values should be approximately equal; however it is clear from Table 2 that the values become larger on passing down the series from M = As to Bi and that there is a very considerable increase on going from $^2K(Sb-Te)$ to $^2K(Bi-Te)$. The causes of this phenomenon are expected to be dominated by the s-electron density terms in the expression for the Fermi contact mechanism (eq 6). The reduced coupling constant method does not take into account the effects of relativity on these s-electron density terms which, as other studies have demonstrated, are extremely important in spin–spin coupling between heavy nuclei.[60,62-64] In the case of Bi in particular, the relativistic effect on the s-electron density is substantial, since with $Z = 83$ it is close to the gold maximum for relativistic effects at $Z = 79$.[65] Previous work on spin couplings in classically bonded Zintl anions has illustrated a method for factoring out the relativistic effects on $|\psi_{ns}(0)|^2$.[63,64] This involves employing the ratio, R^d, of the calculated nonrelativistic and relativistic s-electron densities (eq 9) as a correction factor for each element to give the relativistically corrected reduced coupling constant, $K(AB)_{RC}$, expressed by eq 10.

$$R^d = \left(\frac{|\Psi_{ns}(0)|^2_{nonrel}}{|\psi_{ns}(0)|^2_{rel}}\right) \quad (9)$$

$$K(AB)_{RC} = K(AB)R_A^dR_B^d \quad (10)$$

Values for the nonrelativistic and relativistic s-electron densities (i.e., $|\psi_{ns}(0)|^2_{nonrel}$ and $|\psi_{ns}(0)|^2_{rel}$) were taken from the work of Pykkö and Wiesenfeld[66] and yielded the following ratios: As, 0.8686; Sb, 0.6908; Te, 0.6949; and Bi, 0.2956.

The $^2K(M-Te)_{RC}$ values for the $M(OTeF_5)_6^-$ anions are presented in Table 2 and are much closer in magnitude than the corresponding $^2K(M-Te)$ values. Even so, $^2K(Bi-Te)_{RC}$ is still

(59) Birchall, T.; Myers, R. D.; DeWaard, H.; Schrobilgen, G. J. *Inorg. Chem.* **1982**, *21*, 1068.
(60) Jameson, C. J. In *Multinuclear NMR*; Mason, J., Ed.; Plenum Press: New York, 1987; Chapter 4, p 89.
(61) Pople, J. A.; Santry, D. P. *Mol. Phys.* **1964**, *8*, 1.
(62) Gillespie, R. J.; Granger, P.; Morgan, K. R.; Schrobilgen, G. J. *Inorg. Chem.* **1984**, *23*, 887.
(63) Burns, R. C.; Devereux, L. A.; Granger, P.; Schrobilgen, G. J. *Inorg. Chem.* **1985**, *24*, 2615.
(64) Björgvinsson, M.; Sawyer, J. F.; Schrobilgen, G. J. *Inorg. Chem.* **1987**, *26*, 741.
(65) Pyykkö, P. *Chem. Rev.* **1988**, *88*, 563 and references therein.
(66) Pyykkö, P.; Wiesenfeld, L. *Mol. Phys.* **1981**, *43*, 557.

Table 3. Spin–Lattice Relaxation Times (T_1) and Line Widths ($\Delta\nu_{1/2}$) for the Pnicogen Nuclides in the $M(OTeF_5)_6^-$ Anions (M = As, Sb, or Bi)

$M(OTeF_5)_6^-$	T_1(M), ms	$\Delta\nu_{1/2}$(M)$_{obs}$,[a] Hz	$\Delta\nu_{1/2}$(M)$_{calc}$,[b] Hz	$\Delta\nu_{1/2}$(M)$_{obs}$ – $\Delta\nu_{1/2}$(M)$_{calc}$, Hz
$^{75}As(OTeF_5)_6^-$	2.99	133	106	27
$^{121}Sb(OTeF_5)_6^-$	1.74	212	183	29
$^{123}Sb(OTeF_5)_6^-$	2.49	149	127	22
$^{209}Bi(OTeF_5)_6^-$	1.54	310	207	103

[a] Line width at half-height measured from the spectrum. [b] Line width calculated from $\Delta\nu_{1/2} = (\pi T_1)^{-1}$.

significantly larger than ^2K(As–Te)$_{RC}$ and ^2K(Sb–Te)$_{RC}$. A similar effect has been noted previously for the K_{RC} values in the heaviest members of a congeneric series of species and may be expected since there is still a dependence on the s-electron density.[63] In addition, the value of ^2K(Bi–Te)$_{RC}$ may reflect a difference in the Π_{AB} term. This could arise from differences in the M–O–Te angle in the three anions which might in turn result from changes in the s-character of the M–O and O–Te bonds. Unfortunately, these bond angles are not known for the solution state and the crystal structures of the anions reveal no clear trend in this angle (see later discussion).

(b) ^{75}As, ^{121,123}Sb, and ^{209}Bi Relaxation Study. The experimentally measured half-height line widths for the central pnicogen nuclides in the $M(OTeF_5)_6^-$ anions are given in Table 3. In spite of the local octahedral environment around the central pnicogen nucleus, these line widths are relatively broad and indicate that relaxation is quite fast. The relaxation of quadrupolar nuclei is normally dominated by the highly efficient quadrupolar mechanism described by eq 5, and this is still the case even when the quadrupolar nucleus resides at a site of high electronic symmetry (e.g., T_d or O_h) with an apparent electric field gradient of zero. This occurs because, in solution, small dynamic EFG's are generated by solvation,[67] ion-pair formation,[68] molecular collisions,[69] and asymmetric vibrations[70] of the anion.[70] As alluded to earlier, the ^{75}As line width obtained for $N(CH_3)_4^+As(OTeF_5)_6^-$ in CH_3CN at 30 °C is narrower than the line width ($\Delta\nu_{1/2}$ = 165 Hz) previously obtained for $Cs^+[As(OTeF_5)_6^-]$ in CH_3CN at 25 °C.[31,32] Although the spectra were not obtained at the same temperature, the difference in line widths can more likely be attributed to ion-pair formation, since the ^{75}As spectrum of the Cs^+ salt was obtained from a more concentrated (0.11 M) solution (i.e., higher ion pair concentration) than that for the $N(CH_3)_4^+$ salt. Similar effects have been described for the ^{121}Sb line widths of SbF_6^- and the ^{35}Cl line widths of ClO_4^- salts dissolved in various organic solvents.[71,72]

In order to confirm that the line widths measured from the spectra of the $As(OTeF_5)_6^-$, $Sb(OTeF_5)_6^-$, and $Bi(OTeF_5)_6^-$ anions are attributable to quadrupolar relaxation, the spin–lattice relaxation times (T_1) have been determined. If the relaxation is dominated by the quadrupolar mechanism, then it follows from eq 5 that the line widths calculated from $\Delta\nu_{1/2} = (\pi T_1)^{-1}$ should be equal to the experimentally observed line widths $\Delta\nu_{1/2} = (\pi T_2)^{-1}$. The T_1 values and the line widths calculated from them are presented in Table 3. For ^{75}As, ^{121}Sb, and ^{123}Sb, the calculated line widths are in good agreement with those measured from the spectra, although the difference between the two values reveals that those measured from the spectra are somewhat larger in each case. This difference probably arises from the distortion of the Lorentzian line shape of the central resonance by overlap with the ^{125}Te satellites, thereby producing a larger value for the line width. The dominance of the quadrupolar mechanism can be further confirmed for the ^{121,123}Sb nuclei by considering the ratio $T_1(^{123}Sb)/T_1(^{121}Sb)$, which is proportional to the ratio of the squares of the quadrupole moments (Q) multiplied by the ratio of the spin factors [$f_I = (2I + 3)/(I^2(2I - 1))$] as shown in eq 11.

$$\frac{T_1(^{123}Sb)}{T_1(^{121}Sb)} = \left(\frac{f_I(^{121}Sb)}{f_I(^{123}Sb)}\right)\left(\frac{Q^2(^{121}Sb)}{Q^2(^{123}Sb)}\right) \qquad (11)$$

When the values of $f_I(^{123}Sb)$ and $f_I(^{121}Sb)$ and the quadrupole moments [$Q(^{121}Sb) = -0.28 \times 10^{-28}$ m^2; $Q(^{123}Sb) = -0.36 \times 10^{-28}$ m^2][73] are substituted into eq 11, the ratio $T_1(^{123}Sb)/T_1(^{121}Sb)$ is found to be 1.42. The experimentally determined $T_1(^{123}Sb)$ and $T_1(^{121}Sb)$ values for the $Sb(OTeF_5)_6^-$ anion give a ratio of 1.43 which is in good agreement with the theoretical value.

In contrast, the value of $T_1(^{209}Bi)$ measured for $Bi(OTeF_5)_6^-$ gives a calculated line width which differs from that measured from the spectrum by ~100 Hz. In this case the difference cannot be attributed to the distortion of the Lorentzian line shape of the central ^{209}Bi resonance by overlap with the ^{125}Te satellites, since these are well separated in the spectrum of the $Bi(OTeF_5)_6^-$ anion. The most likely source of the additional broadening is from unresolved long-range coupling of ^{209}Bi to the equatorial fluorine environments of the $OTeF_5$ ligands, i.e., $^3J(^{209}Bi–^{19}F_{eq})$, with a probable magnitude of less than 10 Hz. Three-bond couplings of this type have been previously observed in some other $OTeF_5$ derivatives, viz., $XeF_n(OTeF_5)_{4-n}$,[74] $O{=}XeF_n(OTeF_5)_{4-n}$ where n = 0–3;[74,75] $Te(OTeF_5)_4$,[59] $TeF_2(OTeF_5)^+$,[32] $TeF(OTeF_5)_2^+$,[32] and $TeF_2(OTeF_5)^+$.[32] For such molecules, the three-bond coupling to the axial fluorine environments of the $OTeF_5$ ligands is usually too small to be resolved, although it has been observed for $O{=}Xe(OTeF_5)_4$.[75] In theory the three-bond coupling to F_{eq} in $Bi(OTeF_5)_6^-$ should give rise to a 25-line multiplet; however the broadening from the ^{209}Bi quadrupole relaxation results in only a single broad resonance being observed. The presence of a $^3J(^{209}Bi–^{19}F_{eq})$ coupling is corroborated by the ^{19}F NMR spectrum (*vide infra*) which reveals that the B_4 part of the AB_4 pattern for the $OTeF_5$ ligands is significantly broadened and unresolved, whereas the A part is quite sharp and well resolved.

(c) ^{125}Te NMR Spectra. The ^{125}Te NMR spectra were obtained at elevated temperature (65 °C) in order to reduce the line-broadening effects resulting from the quadrupolar relaxation of the pnicogen nuclides.[56] The ^{125}Te chemical shifts for the $As(OTeF_5)_6^-$ and $Sb(OTeF_5)_6^-$ anions are given in Table 2 and occur in the region typically observed for other $OTeF_5$ derivatives.[32,59,76]

The ^{125}Te NMR spectrum of $N(CH_3)_4^+As(OTeF_5)_6^-$ in CH_3CN (Figure 2a) appears as a sextet of equal-intensity quartets. The quartet splitting (430 Hz) arises from the three-bond coupling of ^{125}Te to ^{75}As and is in good agreement with the value measured from the ^{75}As NMR spectrum. Normally a doublet of quintets would be expected for the coupling of the ^{125}Te to the ^{19}F ligands; however the broadening and overlap of multiplet components which result from the coupling to ^{75}As in this case gives rise to a pseudo-sextet. In addition, the values of $^1J(^{125}Te–^{19}F_A)$ and $^1J(^{125}Te–^{19}F_B)$ measured from the ^{19}F spectrum of $N(CH_3)_4^+As(OTeF_5)_6^-$ in SO_2ClF differ by only 257 Hz (Table 4) and are also expected to be close in value in CH_3CN. The multiplet clearly has an asymmetric appearance which is attributed to higher-order effects. Such effects have been noted previously for other $OTeF_5$ derivatives and arise from the very small difference in chemical shift between the F_A and F_B environments.[76]

The ^{125}Te NMR spectrum of $N(CH_3)_4^+Sb(OTeF_5)_6^-$ in CH_3CN is shown in Figure 2b. Even after accumulation of 425 000

(67) Bryant, R. G. In *NMR of Newly Accessible Nuclei*; Laszlo, P., Ed.; Academic Press: New York, 1983; Vol. 1, p 135.
(68) Hertz, H. G. *Ber. Bunsenges. Phys. Chem.* **1973**, *77*, 531.
(69) Osten, H. J.; Jameson, C. J. *Mol. Phys.* **1986**, *57*, 553.
(70) Doddrell, D. M.; Bendall, M. R.; Healy, P. C.; Smith, G.; Kennard, C. H. L.; Ralston, C. L.; White, A. H. *Aust. J. Chem.* **1979**, *32*, 1219.
(71) Kidd, R. G.; Matthews, R. W. *Inorg. Chem.* **1972**, *11*, 1156.
(72) Cahen, Y. M.; Handy, P. R.; Roach, E. T.; Popov, A. I. *J. Phys. Chem.* **1975**, *79*, 80.
(73) Fuller, G. H. *J. Phys. Chem. Ref. Data* **1976**, *5*, 835.
(74) Schumacher, G. A.; Schrobilgen, G. J. *Inorg. Chem.* **1984**, *23*, 2923.
(75) Jacob, E.; Lentz, D.; Seppelt, K.; Simon, A. *Z. Anorg. Allg. Chem.* **1981**, *472*, 7.
(76) Damerius, R.; Huppmann, P.; Lentz, D.; Seppelt, K. *J. Chem. Soc., Dalton Trans.* **1984**, 2821.

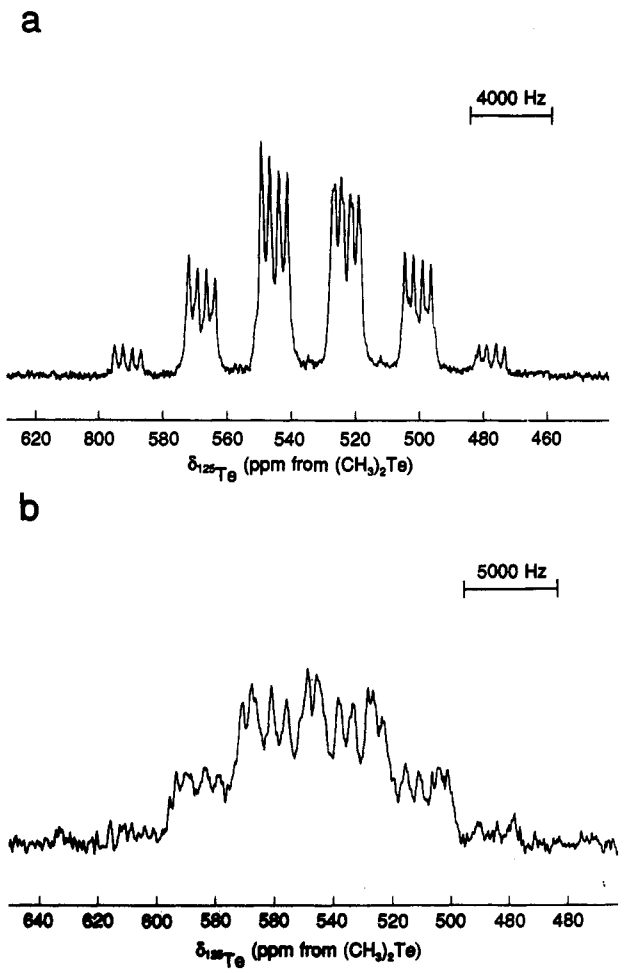

Figure 2. ^{125}Te NMR spectra (157.791 MHz) of the $M(OTeF_5)_6^-$ anions (M = As or Sb) in CH_3CN at 65 °C: (a) $N(CH_3)_4^+As(OTeF_5)_6^-$ (0.05 M); (b) $N(CH_3)_4^+Sb(OTeF_5)_6^-$ (0.08 M).

transients, the signal/noise ratio in this spectrum is low owing to the spread of the intensity over a large number of lines and the broadening of these lines by $^{121,123}Sb$ quadrupolar relaxation. The resonance has a complex multiplet structure which results from the coupling of ^{125}Te to F_A and F_B as well as to the two antimony nuclides ^{121}Sb and ^{123}Sb. The one-bond couplings $^1J(^{125}Te–^{19}F_A)$ and $^1J(^{125}Te–^{19}F_B)$ should give rise to a doublet of quintets, but broadening from the $^{121,123}Sb$ quadrupolar relaxation causes this to appear as a pseudo-sextet. The two-bond couplings $^2J(^{125}Te–^{121}Sb)$ and $^2J(^{125}Te–^{123}Sb)$ will give rise to an equal-intensity sextet and octet, respectively. However, only lines arising from the sextet are readily identifiable since the smaller octet is obscured by the broad components of the sextet. The value of $^2J(^{125}Te–^{121}Sb)$ measured from the spectrum is 800 Hz which is rather larger than the value measured from the ^{121}Sb spectrum. The difference in the values is attributable to quadrupole collapse of the equal-intensity sextet in the ^{125}Te spectrum which results in a symmetrical variation in the spacings between the components of the sextet.[56] Consquently, an accurate value for the $^{125}Te–^{121}Sb$ coupling cannot be extracted from this spectrum without computer simulation.[56] Nevertheless, the value of $^2J(^{125}Te–^{121}Sb)$ measured from the ^{121}Sb spectrum is reliable, since the separation between the ^{125}Te satellites is not influenced by the different lifetimes of the ^{121}Sb spin states.[77]

The ^{125}Te NMR spectrum of the $Bi(OTeF_5)_6^-$ anion would be expected to show a doublet of quintets of equal-intensity decets resulting from the $^1J(^{125}Te–^{19}F_A)$, $^1J(^{125}Te–^{19}F_B)$, and $^2J(^{125}Te–^{209}Bi)$ couplings, respectively. This spectrum could not be obtained owing to the instability of the anion in CH_3CN (*vide infra*) and the long acquisition time that would be required for a spectrum with the intensity spread over such a large number of components.

(d) ^{19}F NMR Spectra. The ^{19}F NMR data for the $As(OTeF_5)_6^-$, $Sb(OTeF_5)_6^-$, and $Bi(OTeF_5)_6^-$ anions are given in Table 4. Each anion gives rise to a single AB_4 pattern characteristic of the $OTeF_5$ group. The chemical shifts and $^2J(^{19}F_A–^{19}F_B)$ values for these resonances all fall within the range found for other $OTeF_5$ derivatives.[78]

The ^{19}F spectrum of the $Sb(OTeF_5)_6^-$ anion has been obtained in three solvents, i.e., SO_2ClF, CH_2Cl_2, and CH_3CN, and the appearance of the spectrum is shown to be solvent dependent. The AB_4 patterns observed for $Sb(OTeF_5)_6^-$ in CH_2Cl_2 and CH_3CN are, even at a field strength of 11.744 T, so severely second order that they have collapsed almost to single lines, thereby indicating that the chemical shifts of F_A and F_B are practically coincident in these solvents. However, in SO_2ClF the frequency separation between $\delta(F_A)$ and $\delta(F_B)$ is sufficiently large to give a reasonably well resolved AB_4 pattern (Figure 3) which could be analyzed and computer simulated in order to extract the value of $^2J(^{19}F_A–^{19}F_B)$. In all three solvents the spectra display ^{125}Te and ^{123}Te satellites flanking the main resonance. These satellites have an asymmetric appearance arising from further second-order effects which are associated with the coupling of the AB_4 spin systems to $^{125,123}Te$ as discussed in the section on the ^{125}Te NMR spectra (*vide supra*).

The ^{19}F NMR spectrum of $Bi(OTeF_5)_6^-$ in SO_2ClF displays an AB_4 pattern in which the A part is well separated from the B_4 part (Figure 4). Interestingly, the B_4 part of the spectrum and its associated $^{125,123}Te$ satellites are noticeably broadened such that the individual transitions are obscured. This broadening is attributed, as discussed earlier, to an extensively quadrupole-collapsed three-bond coupling to ^{209}Bi. In contrast, the lines in the A part of the spectrum are considerably narrower since $^3J(^{19}F_A–^{209}Bi)$ is expected to be very small and hence fully quadrupole collapsed. In addition, the spectrum also reveals a weak AB_4 pattern which is attributable to $F_5TeOTeF_5$ [$\delta(F_A)$, –48.9 ppm; $\delta(F_B)$, –38.9 ppm; $^2J(^{19}F_A–^{19}F_B)$, 182 Hz]. At –40 °C, another AB_4 pattern is observed in addition to the AB_4 pattern $F_5TeOTeF_5$. The new AB_4 pattern is very broad and only the B_4 part [$\delta(F_B)$, –47.4 ppm; $^2J(^{19}F_A–^{19}F_B)$, ~184 Hz] is clearly visible. The observation of these resonances provides evidence for the slow decomposition of the $Bi(OTeF_5)_6^-$ anion in SO_2ClF according to eq 12.

$$Bi(OTeF_5)_6^- \xrightarrow{SO_2ClF,\ 25\ °C} BiO(OTeF_5)_4^- + F_5TeOTeF_5 \qquad (12)$$

This mode of decomposition has been ordered for other $OTeF_5$ derivatives in which there is a central atom in a high oxidation state.[79] It is thought that the broad AB_4 pattern could arise from the new $BiO(OTeF_5)_4^-$ anion and that the broadening of the resonance probably results from ligand exchange. A similar, though much more rapid, decomposition takes place in CH_3CN at 25 °C with the result that a 0.06 M sample has almost completely decomposed within 90 min. The decomposed sample shows resonances attributable to $F_5TeOTeF_5$ and a broad AB_4 pattern [$\delta(F_A)$, –31.4 ppm; $\delta(F_B)$, –41.0 ppm] which is thought to arise from the $BiO(OTeF_5)_4^-$ anion undergoing ligand exchange. In addition, a number of weaker unidentified AB_4 patterns are also observed.

At –40 °C the decomposition of $Bi(OTeF_5)_6^-$ in CH_3CN is slow and the ^{19}F NMR spectrum displays a single AB_4 pattern as expected (Table 4). As in SO_2ClF, the B_4 part of the spectrum is broadened as a result of the extensively quadrupole-collapsed three-bond coupling to ^{209}Bi. In acetonitrile, the chemical shift difference between the F_A and F_B is smaller than in SO_2ClF and consequently the spectrum has more second-order appearance. The smaller chemical shift difference is primarily the result of

(77) Bacon, J.; Gillespie, R. J.; Hartman, J. S.; Rao, U. K. K. *Mol. Phys.* **1970**, *18*, 561.

(78) Seppelt, K. *Z. Anorg. Allg. Chem.* **1973**, *399*, 65.

(79) Seppelt, K. *Angew. Chem., Int. Ed. Engl.* **1982**, *21*, 877.

Table 4. Fluorine-19 NMR Parameters for the $M(OTeF_5)_6^-$ Anions (M = As, Sb, or Bi)

anion[a]	solvent[b]	$\delta(^{19}F)$,[c] ppm	$^2J(^{19}F_A-^{19}F_B)$, Hz	$^1J(^{19}F_A-^{125}Te)$, Hz	$^1J(^{19}F_B-^{125}Te)$, Hz	$^1J(^{19}F_B-^{123}Te)$, Hz
$As(OTeF_5)_6^-$	SO_2ClF	−42.4 (A) −42.0 (B)	188	3370	3627	
$Sb(OTeF_5)_6^-$	SO_2ClF	−42.5 (A) −42.1 (B)	186	3401[d]	3604	2994
	CH_2Cl_2	−41.8[e]	[f]	3556	3624	2951
	CH_3CN	−41.6[e]	[f]	3510	3584	2948
$Bi(OTeF_5)_6^-$	SO_2ClF	−42.4 (A) −40.1 (B)	185	3384	3623	3005
	CH_3CN[g]	−41.1 (A) −39.9 (B)	190	3411	3620	

[a] Data given for solutions (*ca.* 0.05 M) of the $N(CH_3)_4^+$ salts. [b] Recorded at 30 °C unless stated otherwise. [c] A and B refer to the axial and equatorial fluorine environments, respectively, of the $OTeF_5$ ligand. [d] $^1J(^{19}F_A-^{123}Te) = 2778$ Hz. [e] The chemical shifts of the F_A and F_B environments are essentially coincident. [f] The value $^2J(^{19}F_A-^{19}F_B)$ could not be obtained owing to the severely higher-order nature of the spectrum. [g] Recorded at −40 °C.

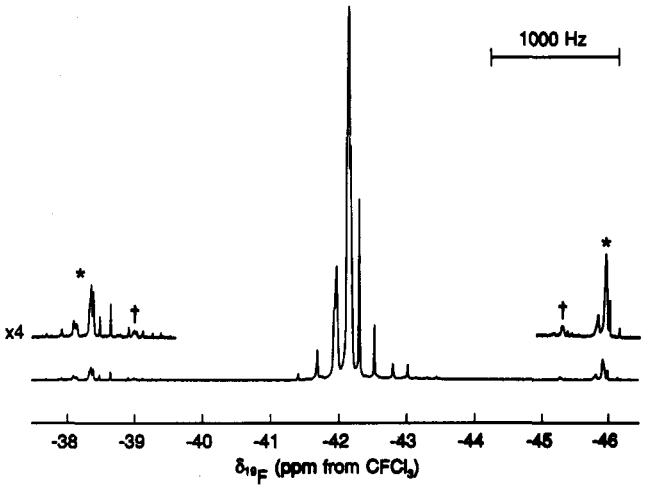

Figure 3. ^{19}F NMR spectrum (470.599 MHz) of $N(CH_3)_4^+Sb(OTeF_5)_6^-$ (*ca.* 0.05 M) in CH_3CN at 30 °C. Asterisks and daggers denote ^{125}Te and ^{123}Te satellites, respectively.

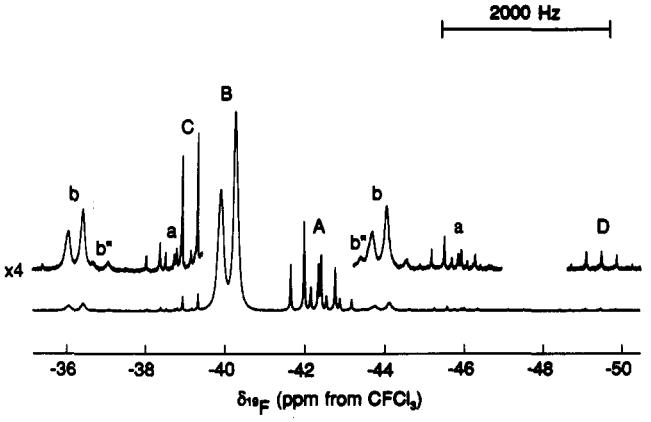

Figure 4. ^{19}F NMR spectrum (470.599 MHz) of $N(CH_3)_4^+Bi(OTeF_5)_6^-$ (*ca.* 0.05 M) in CH_3CN at 30 °C. (A) A part of the AB_4 spectrum of $Bi(OTeF_5)_6^-$. (B) B_4 part of the AB_4 spectrum of $Bi(OTeF_5)_6^-$. Peaks denoted a, b, and b'' indicate satellites resulting from the couplings $^1J(^{19}F_A-^{125}Te)$, $^1J(^{19}F_B-^{125}Te)$, and $^1J(^{19}F_B-^{123}Te)$, respectively. (C) B_4 part of the AB_4 spectrum of $F_5TeOTeF_5$. (D) A part of the AB_4 spectrum of $F_5TeOTeF_5$.

$\delta(F_A)$ moving to higher frequency while $\delta(F_B)$ is much less affected by the change in solvent. The same phenomenon is also observed for the $Sb(OTeF_5)_6^-$ anion when dissolved in CH_2Cl_2 or CH_3CN. An early ^{19}F NMR study of OMF_5 (M = Se or Te) derivatives reported a similar trend in the behavior of $\delta(F_A)$ when the derivatives were dissolved in solvents of higher polarity.[78]

X-ray Crystal Structures of $N(CH_3)_4^+Bi(OTeF_5)_6^-$ (1), $N(CH_3)_4^+As(OTeF_5)_6^-$ (2), $N(CH_2CH_3)_4^+Sb(OTeF_5)_6^-$ (3), and $N(CH_3)_4^+Sb(OTeF_5)_6^-$ (4). Details of the data collection parameters and other crystallographic information are given in Table 5. The final atomic coordinates and the equivalent isotropic thermal parameters are summarized in Tables 13–16 (supplementary material). Parts a–d of Figure 5 show the environments around the As, Sb, and Bi atoms, respectively. Stereoviews of the packing of the unit cells are given in the supplementary material, Figure 8a–d.

The crystal structures consist of well separated tetraalkylammonium cations and $M(OTeF_5)_6^-$ anions. The central pnicogen atoms of the anions are octahedrally coordinated to six oxygen atoms and each of the six tellurium atoms is octahedrally coordinated to an oxygen and five fluorines so that each anion structure can be described as an octahedron of octahedra. Important bond lengths and angles for the $Bi(OTeF_5)_6^-$ (**1**), $As(OTeF_5)_6^-$ (**2**), and $Sb(OTeF_5)_6^-$ (**3** and **4**) anions, together with bond lengths and angles for the $N(CH_3)_4^+$ (**1**, **2**, and **4**) and $N(CH_2CH_3)_4^+$ (**3**) cations are listed in Table 6 and Table 25 (supplementary material) and relevant anion torsion angles are listed in Table 26 (supplementary material). A standard rigid-body librational analysis was performed for all compounds. The corrections were expected to be largest for the light atoms, but as a check, a calculation was also carried out for the heavy atoms. The corrections for libration are not significant for the bismuth anion and one of the arsenic anions (As(2)) (Table 25). For the arsenic (As(1)) anion and the antimony anions of compounds **3** and **4**, the Te–O and Te–F_{eq} distances are significantly affected by thermal motion and, as expected, the librationally corrected Te–O and Te–F bond distances are longer than the uncorrected distances (Table 25) and are in good agreement with other known values.[36,80] The bond lengths corrected for librational motion are also given in Table 6 and Table 25 and are the bond lengths referred to in the following discussion. Each tetraalkylammonium cation is tetrahedral about nitrogen with the expected bond lengths and angles.

(a) $N(CH_3)_4^+Bi(OTeF_5)_6^-$ (1). The required crystallographic symmetry of the anion is $\bar{1}$ with the central bismuth atom on the inversion center, but the actual symmetry is approximately $\bar{3}$. While the anion is perfectly ordered, the cation is subject to a 2-fold positional disorder and gives rise to the superposition of two $N(CH_3)_4^+$ cations in which the central N atoms occupy identical positions. Average $Bi(OTeF_5)_6^-$ anion bond distances are Bi–O = 2.057(6) [2.065] Å (range 2.052(6) [2.058]–2.064(5) [2.072] Å), Te–O = 1.851(6) [1.857] Å (range 1.846(6) [1.852]–1.860(6) [1.864] Å), and Te–F = 1.820(7) [1.833] Å (Te–F_{ax} = 1.822(7) [1.827] Å and Te–F_{eq} = 1.819(7) [1.835] Å). The angles around the central bismuth atoms and the tellurium atoms deviate by a maximum of 5° from the octahedral angles. The angles at the three crystallographically independent oxygen atoms have approximately the same value, ranging from 135.3(3) to 137.1(3)° (Table 6). Little or no information is available in the literature regarding Bi–O bond distances, and to the best of our knowledge, the $Bi(OTeF_5)_6^-$ anion is the first instance where a Bi(V)–O bond length has been determined.

(80) Sawyer, J. F.; Schrobilgen, G. J. *Acta Crystallogr.* **1982**, *B38*, 1561.

Table 5. Summary of Crystal Data and Refinement Results for $N(CH_3)_4^+Bi(OTeF_5)_6^-$ (1), $N(CH_3)_4^+As(OTeF_5)_6^-$ (2), $N(CH_2CH_3)_4^+Sb(OTeF_5)_6^-$ (3), and $N(CH_3)_4^+Sb(OTeF_5)_6^-$ (4)

chemical formula	$C_4H_{12}NO_6F_{30}Te_6Bi$ (1)	$C_4H_{12}NO_6F_{30}Te_6As$ (2)	$C_8H_{20}NO_6F_{30}Te_6Sb$ (3)	$C_4H_{12}NO_6F_{30}Te_6Sb$ (4)
space group	$P\bar{1}$	$R\bar{3}$	$C2/c$	$C2/c$
a (Å)	8.945(2)	10.109(2)	10.506(3)	17.875(3)
b (Å)	9.217(2)	10.109(2)	18.370(6)	10.448(2)
c (Å)	10.029(2)	55.443(17)	20.352(7)	19.752(2)
α (deg)	100.03(3)	90	90	90
β (deg)	99.95(3)	90	91.23(2)	110.83(1)
γ (deg)	98.06(3)	120	90	90
V (Å^3)	789.5	4907	3926.9	3447.8
molecules/unit cell	1	6	4	4
molecular wt (g mol^{-1})	1714.7	1580.7	1683.6	1627.5
calcd density (g cm^{-3})	3.606	3.209	2.848	3.135
T (°C)	−62	24	24	24
μ (cm^{-1})	60.4	34.2	27.7	59.6
λ (Å)	0.56086	0.56086	0.56086	0.71073
R	0.0456	0.0644	0.0548	0.0710
R_w	0.0516	0.0540	0.0461	0.0599

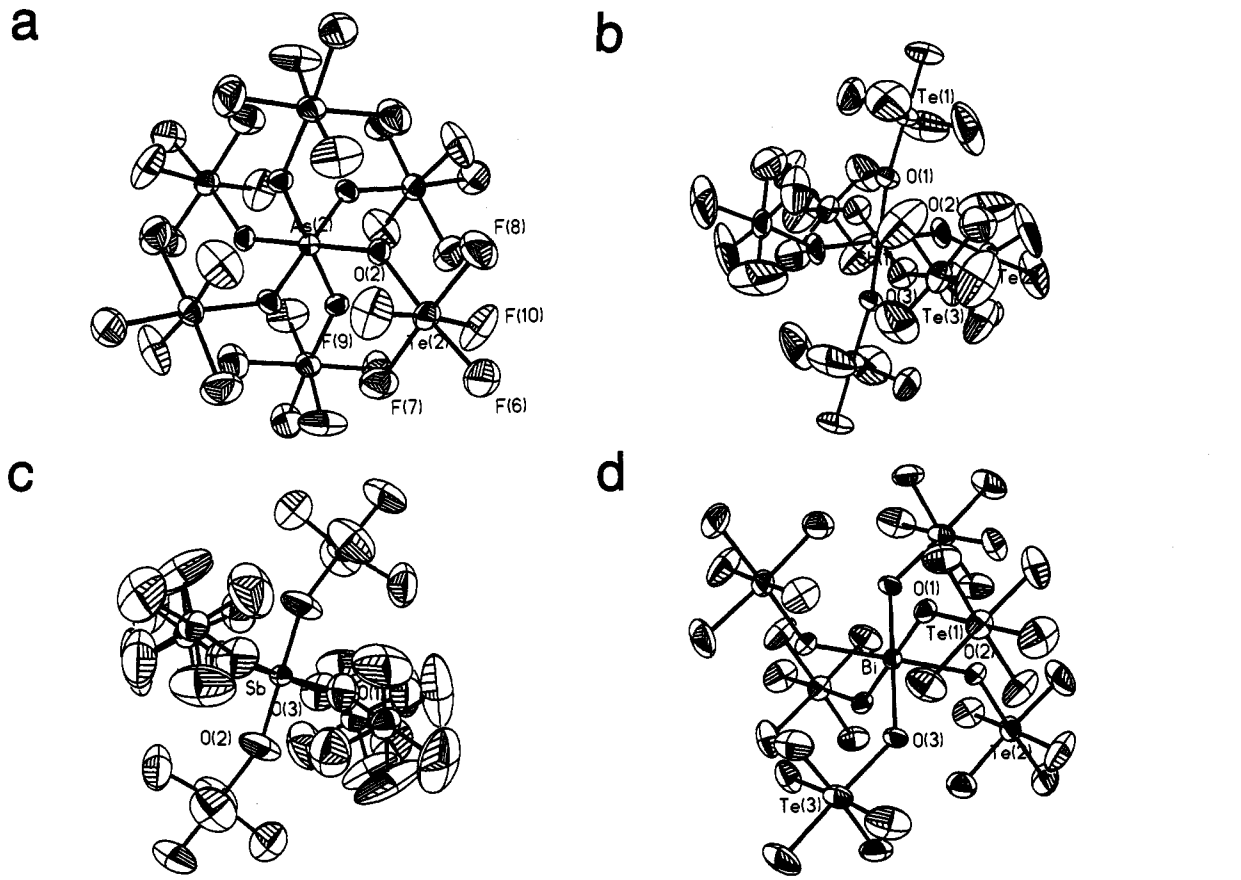

Figure 5. ORTEP views of the anions in (a) $N(CH_3)_4^+As(OTeF_5)_6^-$, (b) $N(CH_3)_4^+Sb(OTeF_5)_6^-$, (c) $N(CH_2CH_3)_4^+Sb(OTeF_5)_6^-$, and (d) $N(CH_3)_4^+Bi(OTeF_5)_6^-$. In the case of the $As(OTeF_5)_6^-$ anion, only one of the two crystallographically equivalent anions corresponding to As(2) is represented. Thermal ellipsoids are shown at the 50% (a and d) and 25% (b and c) probability levels.

While several examples of Bi(III)–O bonds are known, the majority have Bi---O contacts which are greater than the sum of the bismuth and oxygen ionic radii (Bi^{5+}, 0.74 Å; O^{2-}, 1.40 Å). The only other example of a Bi–O bond is the compound $Bi_6(O_4(HO)_4(ClO_4)_6 \cdot 7H_2O$, with a mean Bi(III)–O bond length of 2.15(3) Å.[81]

(b) $N(CH_3)_4^+As(OTeF_5)_6^-$ (2). The central arsenic atoms lie on the rotary inversion centers and the anions have $\bar{3}$ symmetry imposed on them by the lattice. The cation is perfectly ordered and has the expected bond lengths and angles (Table 25). Among the two crystallographically independent anions, one is perfectly ordered while the other one suffers from an orientational disorder along the C_3 axis passing through As(1). This disorder can be described as the superposition of two anions where the As and Te atoms occupy the same positions; their respective thermal parameters are, in fact, very similar to those of As(2) and Te(2) (Table 17, supplementary material). Looking along the C_3 axis, 70% of the $OTeF_5$ groups appear "clockwise", while 30% appear "anticlockwise". The two orientations could be easily resolved for the oxygen atoms, but the large librational motions affecting the fluorine atoms prevented resolution. Taking the disorder into account, the bond distances and angles for the two anions are as follows: As(2)–O(2) = 1.791(9) [1.807] Å, Te(2)–O(2) = 1.860(7) [1.866] Å, Te(2)–F = 1.81(1) [1.84] Å (Te–F_{ax} = 1.849(9) [1.86] Å and Te–F_{eq} = 1.80(1) [1.84] Å), and As(2)–O(2)–Te(2) = 139.9(6)°; As(1)–O(1A) = 1.77(4) Å, As(1)–O(1B) = 1.70(8) Å, Te(1)–O(1A) = 1.87(4) Å, Te(1)–O(1B) = 1.94(7) Å, Te(1)–F = 1.78(2) [1.82] Å (Te–F_{ax} = 1.83(2) [1.83] Å and Te–F_{eq} = 1.77(2) [1.82] Å), As(1)–O(1A)–Te(1) = 141(2)° and As(1)–O(1B)–Te(1) = 140(4)°. Lacking anisotropic parameters for O(1A) and O(1B), the corrected values for

(81) Sundvall, B. *Inorg. Chem.* **1983**, *22*, 1906.

Table 6. Bond Lengths and Bond Angles in $N(CH_3)_4^+Bi(OTeF_5)_6^-$ (1), $N(CH_3)_4^+As(OTeF_5)_6^-$ (2), $N(CH_2CH_3)_4^+Sb(OTeF_5)_6^-$ (3), and $N(CH_3)_4^+Sb(OTeF_5)_6^-$ (4)

Bond Lengths (Å)

$N(CH_3)_4^+Bi(OTeF_5)_6^-$ (1)[a]		$N(CH_3)_4^+As(OTeF_5)_6^-$ (2)[a]	
Bi–O(1)	2.052(6) [2.058]	As(1)–O(1A)	1.77(4)
Bi–O(2)	2.054(6) [2.066]	As(1)–O(1B)	1.70(8)
Bi–O(3)	2.064(5) [2.072]	mean Te–F	1.78(2) [1.82]
mean Te–F	1.820(7) [1.833]	As(2)–O(2)	1.79(3) [1.807]
		mean Te–F	1.81(1) [1.84]
$N(CH_2CH_3)_4^+Sb(OTeF_5)_6^-$ (3)[a]		$N(CH_3)_4^+Sb(OTeF_5)_6^-$ (4)[a]	
Sb–O(1)	1.87(1) [1.92]	Sb–O(1)	1.92(1) [1.99]
Sb–O(2)	1.87(1) [1.91]	Sb–O(2)	1.90(1) [1.96]
Sb–O(3)	1.88(2) [1.91]	Sb–O(3)	1.90(1) [1.93]
mean Te–F	1.71(2) [1.80]	mean Te–F	1.75(2) [1.85]

Bond Angles (deg)

$N(CH_3)_4^+Bi(OTeF_5)_6^-$ (1)		$N(CH_3)_4^+As(OTeF_5)_6^-$ (2)	
Bi–O(1)–Te(1)	137.1(3)	As(1)–O(1)–Te(1)	141(2)
Bi–O(2)–Te(2)	135.7(3)	As(1)–O(1B)–Te(1B)	140(4)
Bi–O(3)–Te(3)	135.3(3)	As(2)–O(2)–Te(2)	139.9(6)
$N(CH_2CH_3)_4^+Sb(OTeF_5)_6^-$ (3)		$N(CH_3)_4^+Sb(OTeF_5)_6^-$ (4)	
Sb–O(1)–Te(1)	160.7(9)	Sb–O(1)–Te(1)	148.4(8)
Sb–O(2)–Te(2)	160.8(9)	Sb–O(2)–Te(2)	150.9(7)
Sb–O(3)–Te(3)	167(1)	Sb–O(3)–Te(3)	153.4(8)

[a] Distances after corrections for thermal motion by the riding model are given in square brackets.

their bond lengths with As(1) and Te(1) are not reported. The As–O bond lengths are comparable to normal As(V)–O bond lengths found in $M_2(As_2F_{10}O)\cdot H_2O$ (M = Rb: As–O = 1.75 Å; M = K: As–O = 1.74 Å),[82] and $M_2(As_2F_8O_2)$ (M = K: As–O = 1.816 Å; M = Rb: As–O = 1.811 Å; M = Cs: As–O = 1.790 Å),[83] in which As is hexacoordinated.

(c) $N(CH_2CH_3)_4^+Sb(OTeF_5)_6^-$ (3) and $N(CH_3)_4^+Sb(OTeF_5)_6^-$ (4). The required crystallographic symmetry of the anion is $2/m$ with the central antimony atom on the inversion center, but the actual symmetry is almost $\bar{3}$ as in the bismuth compound. The cations have the expected bond lengths and angles (Table 25). The average bond distances for the anion in compound **3** are Sb–O = 1.87(1) [1.91] Å (range 1.87(1) [1.92]–1.88(2) [1.91] Å), Te–O = 1.74(1) [1.76] Å (range 1.72(2) [1.73]–1.75(1) [1.78] Å), Te–F = 1.71(2) [1.80] Å (Te–F_{ax} = 1.76(2) [1.79] Å and Te–F_{eq} = 1.70(2) [1.80] Å), and the bond angle is Sb–O–Te 162.8(9)° (range 160.7(9)–167(1)°). In compound **4**, the average bond distances are Sb–O = 1.91(1) [1.96] Å (range 1.90(1) [1.93]–1.92(1) [1.99] Å), Te–O = 1.78(1) [1.81] Å (range 1.76(1) [1.80]–1.787(9) [1.810] Å), Te–F = 1.75(2) [1.85] Å (Te–F_{ax} = 1.79(2) [1.83] Å and Te–F_{eq} = 1.74(2) [1.85] Å), and the Sb–O–Te bond angle is 150.9(8)° (range 148.4(8)–153.4(8)°). Even though the two compounds crystallized in the same space group, the structures of the two anions are not identical. As expected, the Sb–O, Te–O, and Te–F bond lengths are very similar, but the Sb–O–Te angles differ by more than 10° (*vide infra*). In both compounds, and as previously observed in the case of the $U(OTeF_5)_6$ molecule,[84] the fluorine and oxygen atoms have exceptionally large thermal parameters showing the pentafluorotellurate groups are undergoing angular motions of large amplitude. Consequently, the Te–O and Te–F distances are significantly affected by this thermal motion (see the values obtained before and after corrections for libration compared to those obtained in the bismuth and arsenic anions). However, the Sb–O distances found can be compared with the Sb(V)–O distances of 1.92 Å in $Cs_3Sb_3F_{12}O_3$[85] and 1.91 Å in $Rb_2(Sb_2F_{10}O)$,[86] where the Sb atoms are also octahedrally coordinated to O atoms.

Structural Comparison among the $M(OTeF_5)_6^-$ Series of Anions and Related Derivatives. The six $OTeF_5$ groups have ample space to fit together without suffering any significant distortion from their normal pseudo-octahedral geometry. All distances between atoms of neighboring $OTeF_5$ groups are longer than the sum of the corresponding van der Waals radii for two fluorines (2.70–2.80 Å[87,88]). The closest F···F contacts within $OTeF_5$ groups compared with the closest F···F contacts between neighboring $OTeF_5$ groups are the following: $As(OTeF_5)_6^-$ [2.449–2.534, 3.055–3.876 Å], $Sb(OTeF_5)_6^-$ [2.321–2.437, 2.782–3.998 Å ($N(CH_3)_4^+$); 2.240–2.456, 3.067–3.972 Å ($N(CH_2CH_3)_4^+$)], $Bi(OTeF_5)_6^-$ [2.505–2.546, 2.966–3.241 Å], respectively. As already observed in many other structures containing the $OTeF_5$ groups, the Te–F_{eq} and Te–F_{ax} bond lengths are very similar and are indistinguishable based on bond length differences as these differences lie within the ranges of the standard deviations. Moreover, this also appears to be true in solution where the resonances associated with the F_{eq} and F_{ax} environments in the ^{19}F NMR spectra are generally very strongly coupled and exhibit severe second-order effects (see section on NMR spectroscopy). The average Te–O and average Te–F bond distances are comparable to those found in many $OTeF_5$ compounds such as in the related compounds (and isoelectronic with $Sb(OTeF_5)_6^-$) $Te(OTeF_5)_6$ (Te–O = 1.896(4) Å; Te–F = 1.817(4) Å),[36] $B(OTeF_5)_3$ (Te–O = 1.874(6) Å; Te–F = 1.816(5) Å),[80] and $B(OTeF_5)_4^-$ (Te–O = 1.78(1) – 1.858(5) Å; Te–F = 1.803(7)–1.860(5) Å).[28] In the bismuth and arsenic structures, the average Te–O distances [1.857, 1.866 Å] are slightly longer than their average Te–F distances [1.833, 1.84 Å] while in the antimony structures the average Te–O distances [1.76/1.81 Å] are slightly shorter than their average Te–F distances [1.80/1.85 Å], but again, the differences lie within the range of the standard deviations and are not significant. The $OTeF_5^-$ anion is the only case where the Te–O bond [1.803 Å] has been found to be significantly shorter than the average Te–F bond [1.871 Å].[89]

Among the most interesting aspects of these four related anion structures are variations of the M–O bond lengths, M–O–Te angles and O′–M–O–Te torsion angles. As expected, the average M–O bond distances increase in the order As–O < Sb–O < Bi–O [1.807 Å < 1.91/1.96 Å < 2.065 Å], and are in good agreement with the sums of the O^{2-} and pnicogen(+5) ionic radii (As^{5+}, 0.47 Å; Sb^{5+}, 0.62 Å; Bi^{5+}, 0.74 Å; O^{2-}, 1.40 Å)[90] and, in the case of antimony compounds **3** and **4**, are independent of the countercation. In the sterically less congested $B(OTeF_5)_3$ and $B(OTeF_5)_4^-$ species, the B–O–Te angles are 132.3(4)° and 128.3(7)–133.4(7)°, respectively. The M–O–Te angles are all greater than those of boron species, and it is clear that the $OTeF_5$ groups in the octahedral $M(OTeF_5)_6^-$ anions and related octahedral $OTeF_5$ derivatives do not suffer serious steric congestion (*vide supra*) because congestion is relieved by overall increases in the M–O–Te angles. Seppelt and co-workers[91] have recently noted that in a series of neutral $M(OTeF_5)_6$ derivatives, the M–O–Te angle should be strongly influenced by steric considerations, and that the M–O–Te angle could be expected to decrease with increasing atomic number. The present experimental findings make such correlations less certain, at least when extended to salts, as only a slight decrease in the average M–O–Te angle is observed upon going from As (140(2)°) to Bi (136.2(3)°), whereas the Sb–O–Te angles of both the $N(CH_3)_4^+$ (150.9(8)°) and $N(CH_2CH_3)_4^+$ (162.8(9)°) salts are significantly larger than in their arsenic and bismuth analogs. Moreover, the Sb–O–Te angles in $N(CH_2CH_3)_4^+Sb(OTeF_5)_6^-$ and $N(CH_3)_4^+Sb(OTeF_5)_6^-$ are at considerable variance when compared to each other and with the

(82) Haase, von W. *Acta Crystallogr.* **1974**, *B30*, 1722.
(83) Haase, von W. *Chem. Ber.* **1974**, *107*, 1009.
(84) Templeton, L. K.; Templeton, D. H.; Bartlett, N.; Seppelt, K. *Inorg. Chem.* **1976**, *15*, 2720.
(85) Haase, von W. *Acta Crystallogr.* **1974**, *B30*, 2465.
(86) Haase, von W. *Acta Crystallogr.* **1974**, *B30*, 2508.
(87) Pauling, L. *The Nature of the Chemical Bond*, 3rd ed.; Cornell University Press: Ithaca, NY, 1960; p 260.
(88) Bondi, A. *J. Phys. Chem.* **1964**, *68*, 441.
(89) Miller, P. K.; Abney, K. D.; Rappé, A. K.; Anderson, O. P.; Strauss, S. H. *Inorg. Chem.* **1988**, *27*, 2255.
(90) Pauling, L. *The Nature of the Chemical Bond*, 3rd ed.; Cornell University Press: Ithaca, NY, 1960; p 514.
(91) Turowsky, L.; Seppelt, K. *Z. Anorg. Allg. Chem.* **1990**, *590*, 23.

values of the isoelectronic Te compound, $Te(OTeF_5)_6$ (138.9(2)–139.1(2)°). Seppelt and co-workers[91] have noted that the M–O–Te angles in the neutral $Te(OTeF_5)_6$,[36] $Mo(OTeF_5)_6$,[91] and $U(OTeF_5)_6$[84] molecules differ markedly from one another (U–O–Te angles, 170(2)–171(1)°; Mo–O–Te angles, 145.6(2)–146.2(2)°) and have attributed the differences to considerable M–O double bond character, which is underscored by the anticipated decrease in steric crowding which would otherwise induce the opposite effect in the U–O–Te angle. Although the large U–O–Te angle in $U(OTeF_5)_6$ is likely attributable to U–O double bond character, the present study indicates that caution must be exercised when making comparisons among octahedral $OTeF_5$ derivatives which involve steric considerations. There is no simple trend in the variation of the M–O–Te angles among $Te(OTeF_5)_6$ and its pnicogen anion analogs and it appears these angles are, in large measure, determined by packing considerations. The variation observed in the Sb–O–Te angle by changing the nature of the countercation alone establishes that the M–O–Te angles, in large measure, depend on the packing and not solely on the nature of the M atom.

The lattice packings of compounds containing the $N(CH_3)_4^+$ cation can reasonably be expected to be dominated by the large anions. The *trans*-$OTeF_5$ groups in compounds **1**–**4** are symmetry related so that the M–O–Te–F_a arrangements are *trans* to one another and have *anti*-conformations (cf. O′–M–O–Te torsion angles; Table 26), consequently, the effective diameters of the anions are given by the $F_{ax}\cdots F_{ax}$ distance for any pair of *trans*-$OTeF_5$ groups plus twice the van der Waals radius of fluorine (average value, 1.38 Å[87,88]). The effective anion radii estimated in this manner are similar for the arsenic and antimony anions: $N(CH_3)_4^+As(OTeF_5)_6^-$, 5.92 Å; $N(CH_3)_4^+Sb(OTeF_5)_6^-$, 6.01 Å; $N(CH_2CH_3)_4^+Sb(OTeF_5)_6^-$, 6.00 Å; $N(CH_3)_4^+Bi(OTeF_5)_6^-$, 6.74 Å. The crystal structures of $N(CH_3)_4^+As(OTeF_5)_6^-$ and $N(CH_3)_4^+Sb(OTeF_5)_6^-$ are clearly dominated by the large sizes of the anions and consist of cubic closest packed anion lattices with the cations occupying octahedral interstital anion lattice sites (cf. cation/anion radius ratios of 0.59 and 0.58, respectively, based on an estimated effective radius for the $N(CH_3)_4^+$ cation of 3.48–3.50 Å). Although the cation/anion radius ratio of $N(CH_3)_4^+Bi(OTeF_5)_6^-$ (0.52) is conducive to a closest packed anion lattice, the crystal packing is best described as two interpenetrating cubic closest packed lattices of cations and anions so that it is near closest packed and equivalent to a body centered cubic lattice in which both the cation and anion are in cuboctahedral environments of their counterions. The $N(CH_2CH_3)_4^+Sb(OTeF_5)_6^-$ lattice is not closest packed. The counterion environment of the cation is a trigonal prism and that of the anion is an octahedron. A comparison of the molecular volumes, V/Z, shows a near linear increase in M–O–Te angle with increasing V/Z in the order $N(CH_3)_4^+Bi(OTeF_5)_6^- < N(CH_3)_4^+As(OTeF_5)_6^- < N(CH_3)_4^+Sb(OTeF_5)_6^- < N(CH_2CH_3)_4^+Sb(OTeF_5)_6^-$ and is consistent with the crystal lattice descriptions. The small Bi–O–Te angles in $Bi(OTeF_5)_6^-$ are likely a consequence of the large covalent radius of bismuth. Presumably the reduced congestion about bismuth allows the Bi–O–Te angles to approach the B–O–Te angles of $B(OTeF_5)_3$ and $B(OTeF_5)_4^-$ and aids in producing the most efficient packing arrangement among the series of $M(OTeF_5)_6^-$ anions. The large cation/anion ratio of $N(CH_2CH_3)_4^+Sb(OTeF_5)_6^-$ (0.74–0.76, based on an effective $N(CH_2CH_3)_4^+$ radius of 4.47–4.56 Å) leads to a non-closest-packed lattice and is consistent with the view that crystal packing, in large measure, determines why the Sb–O–Te angle (162.8(9)°) in this structure is larger than in the cubic closest packed structure of $N(CH_3)_4^+Sb(OTeF_5)_6^-$ (150.9(8)°).

Although the $Bi(OTeF_5)_6^-$ anion is the largest of the series, the V/Z ratio is the smallest, making it the most efficiently packed compound in the series. Consequently, the closest anion–cation contacts occur in $N(CH_3)_4^+Bi(OTeF_5)_6^-$ with the closest anion–cation distance occurring between F(7) and C(2A) [2.77(3) Å] and F(14) and C(4A) [2.75(2) Å] whereas the remaining closest F···C distances occur at 3.228 (F(4)···C(1)), 3.134 (F(C10)···C(3)), and 3.229 Å (F(5)···C(1)) (Figure 7), supplementary material). The sum of the van der Waals radii of CH_3 (2.00 Å)[87] and F (1.35[87] – 1.40[88] Å) is 3.35–3.40 Å. The F(7)···C(2A) and F(14)···C(4A) distances suggest a significant degree of hydrogen bonding between the C(2A) and C(4A) methyl groups and F(7) and F(14) atoms. In the arsenic and antimony compounds, the closest anion–cation distances occur between F(4) and C(1) [3.243 Å] and F(7) and C(4) [3.295 Å], respectively, in the $N(CH_3)_4^+$ compounds and between F(7) and C(4A) [3.268 Å] and F(6) and C(2) [3.512 Å] for $N(CH_2CH_3)_4^+Sb(OTeF_5)_6^-$, which are at the limit of the $CH_3\cdots F$ van der Waals distance (3.35–3.40 Å). It appears that the hydrogen bond interactions between the $N(CH_3)_4^+$ cation and $Bi(OTeF_5)_6^-$ anion serve to constrain librational motions of the fluorine and oxygen atoms, producing correspondingly smaller thermal parameters than in the arsenic and antimony structures (Tables 17–20 and Figure 5a, supplementary material).

Table 26 gives the symmetry-related pairs of O′–M–O–Te torsion angles for the $M(OTeF_5)_6^-$ anions. Each torsion angle is defined relative to two orthogonal planes of oxygen atoms containing the O′–M–O moieties. Twelve torsion angles need to be defined for the bismuth and antimony anions since there are three crystallographically independent $OTeF_5$ groups for each of them, whereas only four torsion angles need to be defined in the arsenic case since there is only one crystallographically independent $OTeF_5$ group in this anion. As a result of their symmetry equivalence, the torsion angles associated with the $OTeF_5$ groups trans to one another are identical.

The torsion angles of the three crystallographically independent $OTeF_5$ groups in the bismuth anion are identical within experimental error. Moreover, the torsion angles in the bismuth and arsenic anions are very similar, i.e., the smallest average torsion angles relative to each reference plane are 29.5(5)° and 33(1)°, respectively, and are comparable to the average minimum torsion angle found in $Te(OTeF_5)_6$, 27(3)°. In both the bismuth and arsenic anions the O′–M–O–Te torsion angles produce regular environments around the metal atom, i.e., the minimum torsion angle is related to any other torsion angle by ±90 or ±180°. Other than their symmetry-related pairing, the O′–M–O–Te torsion angles in both antimony compounds are in marked contrast to those of the arsenic and bismuth analogs and are found to be irregular. As can be seen from Table 26, the minimum torsion angles with respect to a given reference plane for $N(CH_3)_4^+Sb(OTeF_5)_6^-$ and $N(CH_2CH_3)_4^+Sb(OTeF_5)_6^-$ range from 3 to 66° and from 24 to 66°, respectively, and are not simply related.

Until the present study, the $Ti(OTeF_5)_6^{2-}$ anion in $[Ag(CH_2Cl_2)_3]_2^{2+}Ti(OTeF_5)_6^{2-}$ [30] was the only other example of a hexakis(pentafluorooxotellurate) anion which had been characterized by single-crystal X-ray diffraction. Although the anion is divalent and expected to be more basic than the monovalent series of pnicogen anions, there are no contacts between Ag^+ and the oxygens of the $OTeF_5$ groups. Rather, the coordination sphere of silver is occupied by Ag–Cl contacts with the solvent and long Ag···F contacts with the anion. It is readily apparent from a comparison of the Ti–O bond lengths (1.933(6)–1.939(9) Å) and Ti–O–Te angles (142.3(4)–145.2(5)°) with the corresponding parameters of the $As(OTeF_5)_6^-$ anion (As–O = 1.70(8)–1.791(9) Å; As–O–Te = 139.9(6)–141(2)°) that the oxygen electron lone pairs are less accessible in the arsenic anion. The $As(OTeF_5)_6^-$ is expected to function as a better least coordinating anion than $Ti(OTeF_5)_6^{2-}$ on the basis of steric and formal charge criteria (*vide supra*). While $Ti(OTeF_5)_6^{2-}$ and $Sb(OTeF_5)_6^-$ (Sb–O = 1.91–1.96 Å; Sb–O–Te = 160.7(9)–167(1)°, 148.4(8)–153.4(8)°) rank about equal in terms of size and access to oxygen electron lone pairs, the antimony anion, like $As(OTeF_5)_6^-$, is expected to be a poorer $OTeF_5^-$ donor than $Ti(OTeF_5)_6^{2-}$ and to be less fluorobasic owing to its univalent character and larger

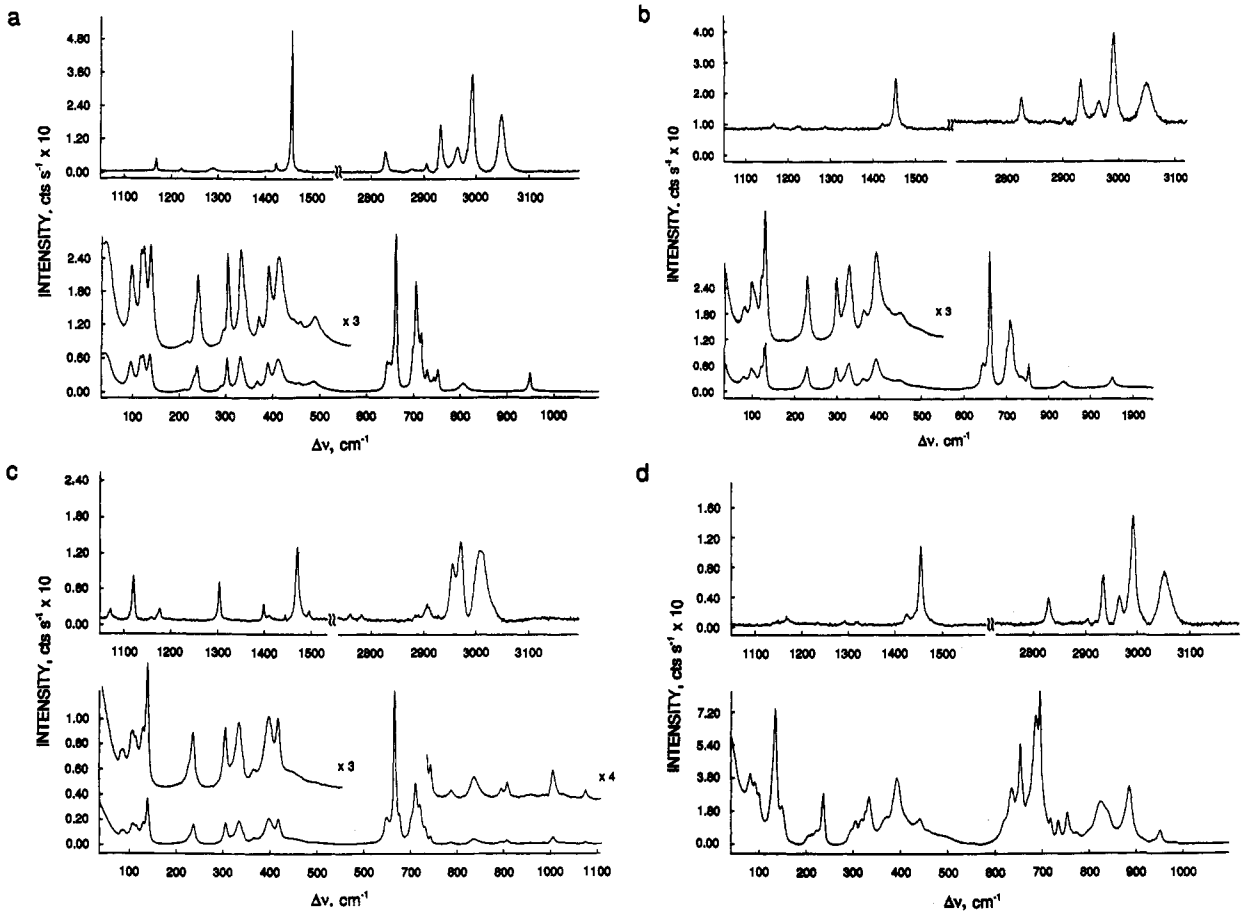

Figure 6. Raman spectra of microcrystalline (a) $N(CH_3)_4^+As(OTeF_5)_6^-$ (**2**), (b) $N(CH_3)_4^+Sb(OTeF_5)_6^-$ (**4**), (c) $N(CH_2CH_3)_4^+Sb(OTeF_5)_6^-$ (**3**), and (d) $N(CH_3)_4^+Bi(OTeF_5)_6^-$ (**1**) recorded in glass capillaries at room temperature using 514.5-nm excitation.

size. It is anticipated, based on a consideration of the relative fluoride ion base strengths of AsF_6^-, SbF_6^-, and BiF_6^- and the relative charge-to-radius ratios that the largest anion, $Bi(OTeF_5)_6^-$, is the weakest $OTeF_5^-$ ion donor and least basic of all. However, the greater Bi–O bond lengths (2.058–2.072 Å) and smaller Bi–O–Te bond angles (135.3(3)–137.1(3)°) suggest that the oxygen atoms of $Bi(OTeF_5)_6^-$ are actually more available for coordination than those of $As(OTeF_5)_6^-$ and $Sb(OTeF_5)_6^-$.

Raman Spectra of $N(CH_3)_4^+Bi(OTeF_5)_6^-$ (1), $N(CH_3)_4^+As(OTeF_5)_6^-$ (2), $N(CH_2CH_3)_4^+Sb(OTeF_5)_6^-$ (3), and $N(CH_3)_4^+Sb(OTeF_5)_6^-$ (4). The solid-state Raman spectra of the title compounds are shown in Figure 6. The observed frequencies and their assignments are summarized in Table 7. Spectral assignments are necessarily tentative owing to uncertainties regarding the degree of vibrational coupling among the $OTeF_5$ modes of the ligands, anticipated strong coupling among vibrational modes associated with the M–O–Te moieties, and the degrees of site symmetry lowering, as well as vibrational coupling within the unit cells (factor-group splitting). The assignments of the frequencies of the $OTeF_5$ groups have been aided by comparison with the most recent assignments for $N(CH_3)_4^+TeOF_5^-$,[92] for which *ab initio* calculations and a normal coordinate analysis confirm the correctness of the assignments, and by assignments for F_5TeOF.[93] Assignments were made under C_{4v} symmetry for the $OTeF_5$ group which has 15 vibrations, $4A_1 + 2B_1 + B_2 + 4E$, all of which are Raman active (A_1 and E are infrared active), and generally require no further comment.

Modes corresponding to the M–O and Te–O stretching modes are expected to be strongly vibrationally coupled as a result of the large masses of the pnicogen and tellurium atoms and are expected to be intense in the Raman spectra. These modes have been assigned by comparison with the strongly coupled and intense Xe–O and Te–O modes in $Xe(OTeF_5)_2$ (428, 442 cm^{-1}),[94] $FXeOTeF_5$ (475 cm^{-1}),[87] and $XeOTeF_5^+$ (487 cm^{-1}).[94] The assignments of the M–O–Te bends have also been made by comparison with those of $Xe(OTeF_5)_2$ (133 cm^{-1})[94] and $XeOTeF_5^+$ (174 cm^{-1}).[94] The M–O–Te torsions are assigned to moderately intense low-frequency bands at 80–130 cm^{-1}, but are more tenuous.

The assignments for the $N(CH_3)_4^+$ cations are based on those for the free $N(CH_3)_4^+$ cation, which belongs to the point group T_d and has 19 fundamental vibrations, $3A_1 + A_2 + 4E + 4T_1 + 7T_2$. Of these, the T_2 modes are infrared active and A_1, E, and T_2 modes are Raman active. Although the assignments for the $N(CH_3)_4^+$ cations generally follow those previously given for other $N(CH_3)_4^+$ salts[96-101] and require little further comment, they do exhibit some interesting features. Explicit assignments for the $N(CH_2CH_3)_4^+$ cation are not given for $N(CH_2CH_3)_4^+Sb(OTeF_5)_6^-$, but the frequencies are listed in Table 7 opposite related $N(CH_3)_4^+$ vibrational modes.

A previous study by Kabisch[99] of the deviations of the Raman spectra of the free $N(CH_3)_4^+$ cation from the T_d selection rules in various salts of known crystal structures has provided empirical rules for estimating, from vibrational spectra, the degree of $N(CH_3)_4^+$ cation distortion. Changes in the methyl stretching and second-order bands, whose intensities are enhanced due to Fermi resonance (3050–2750 cm^{-1}), and methyl deformation

(92) Christe, K. O.; Dixon, D. A.; Sanders, J. C. P.; Schrobilgen, G. J.; Wilson, W. W. *Inorg. Chem.* **1993**, *32*, 4089.
(93) Schack, C. J.; Wilson, W. W.; Christe, K. O. *Inorg. Chem.* **1983**, *22*, 18.
(94) Schrobilgen, G. J.; Keller, N. *Inorg. Chem.* **1981**, *20*, 2118.
(95) Sladky, F. *Monatsh. Chem.* **1970**, *101*, 1571.
(96) Berg, R. W. *Spectrochim. Acta, Part A* **1978**, *34A*, 655.
(97) Bottger, G. L.; Geddes, A. L. *Spectrochim. Acta* **1978**, *21*, 1708.
(98) Kabisch, G.; Klose, M. J. *Raman Spectrosc.* **1978**, *7*, 312.
(99) Kabisch, G. *Raman Spectrosc.* **1980**, *9*, 279.
(100) Wilson, W. W.; Christe, K. O.; Feng, J.; Bau, R. *Can. J. Chem.* **1989**, *67*, 1898.
(101) Christe, K. O.; Wilson, W. W.; Wilson, R. D.; Bau, R.; Feng, J. *J. Am. Chem. Soc.* **1990**, *112*, 7619.

Table 7. Raman Frequencies and Assignments for $N(CH_3)_4^+As(OTeF_5)_6^-$, $N(CH_3)_4^+Sb(OTeF_5)_6^-$, $N(CH_2CH_3)_4^+Sb(OTeF_5)_6^-$, and $N(CH_3)_4^+Bi(OTeF_5)_6^-$ [a]

freq, cm^{-1}				assignments	
$N(CH_3)_4^+As(OTeF_5)_6^-$	$N(CH_3)_4^+Sb(OTeF_5)_6^-$	$N(CH_2CH_3)_4^+Sb(OTeF_5)_6^-$ [b]	$N(CH_3)_4^+Bi(OTeF_5)_6^-$	cation	anion
3049(7)	3050(12)		3052(8)	$\nu_5(E)$, $\nu_{as}(CH_3)$; $\nu_{13}(T_2)$, $\nu_{as}(CH_3)$	
2992(13)	2991(24)	3008(10)	2993(19)	$\nu_1(A_1)$, $\nu_s(CH_3)$	
2965(3)	2965(7)	2970(11)	2966(5)	$\nu_{14}(T_2)$, $\nu_{as}(CH_3)$	
		2955(8)			
2932(6)	2933(12)		2935(8)	$2\nu_6(E)$, $2\nu_2(A_1)$	
2905(<1)	2905(2)	2907(2)	2906(1)		
2876(<1)		2880(<1)		$\nu_6(E) + \nu_{16}(T2)$	
2827(3)	2827(7)		2830(4)	$2\nu_{16}(T_2)$	
		2783(<1)			
		2761(1)			
1454(18)	1453(9)	1467(10)	1454(13)	$\nu_2(A_1)$, $\delta(CH_3)$; $\nu_6(E)$, $\delta_{as}(CH_3)$	
1422(1)			1425(2)	$\nu_{16}(T_2)$, $\delta_{as}(CH_3)$	
		1398(2) [b]			
1289(<1)		1304(5)		$\nu_{17}(T_2)$, $\delta_{rock}(CH_3)$	
1221(<1)				?	
1169(2)		1177(2), 1121(6), 1072(1), 1002(4) [b]	1170(1)	$\nu_7(E)$, $\delta_{rock}(CH_3)$	
			983(1)	?	
948(12)	948(8)		952(9)	$\nu_{18}(T_2)$, $\nu_{as}(CN_4)$	
		906(2)			
		893(2)			
			887(38)		
	833(5)	835(3)	839(23), sh [c]		
			827(28)		
806(5)			803(10)		
		786(<1)	773(8)	$\nu_3(A_1)$, $\nu_s(CN_4)$	
751(14)	751(18)		754(21)		
742(9)	737(8)	742(5)			$\nu_8(E)$, $\nu_{as}(TeF_4)$
728(14)	731(9)	729(11)	735(16)		
715(37)	722(11), sh	719(25)	719(17)		
704(70)	706(50)	709(40)			$\nu_1(A_1)$, ν(TeF)
		700(20)	697(100)		
			689(84)		
		675(20)			$\nu_2(A_1)$, $\nu_s(TeF_4)$
660(100)	659(100)	666(100)	655(65)		
648(18)					
642(19)	643(18)	647(18)	635(37)		$\nu_5(B_1)$, $\nu_{as}(TeF_4)$
			622(16), sh		?
487(7)					
457(6)	453(7)	450(4)		$\nu_{19}(T_2)$, $\delta(CN_4)$	
443(6)			440(17)		$\nu_3(A_1)$, ν(Te–O) strongly coupled with ν(M–O)
414(21)	426(8)	419(16)			
392(19)	397(22)	399(17)	393(43)		
370(7)	367(8)	369(4)	370(15)	$\nu_8(E)$, $\delta(CN_4)$	
334(22)	334(19)	336(15)	333(28)		$\nu_9(E)$, $\delta(FTeF_4)$;
			326(21), sh		
			317(16)		$\nu_{10}(E)$, $\delta(OTeF_4)$
306(33)	304(16)	308(14)	305(16)		$\nu_4(A_1)$, $\delta_s(FTeF_4)$
295(6), sh			297(10), sh		
242(17)		240(13)			$\nu_7(B_2)$, $\delta_{acias}(TeF_4)$
237(10), sh	236(16)		236(33)		
218(2)			223(9)		$\nu_{11}(E)$, $\delta_{as}(TeF_4)$
			208(6)		
			148(25)		δ(TeOM)
143(24)	139(34)	142(29)	134(89)		
129(23)	130(17), sh	133(14)			
124(23)		118(12), sh			
103(19)	108(15)	110(13)	99(33)	lattice modes + τ(TeOM)	
	90(9)	89(9)	90(40)		
			81(46)		

[a] Spectra were recorded on microcrystalline powders in Pyrex glass melting point capillaries at room temperature using 514.5-nm excitation; values in parentheses denote relative intensities and sh denotes a shoulder. [b] Bands associated with the $N(CH_2CH_3)_4^+$ cation cannot be assigned in all cases. [c] No assignments have been made for the bands in this region which are tentatively attributed to Fermi resonance enhanced overtones of the strongly coupled M–O–Te stretching modes.

(1150–1470 cm^{-1}) bands are particularly diagnostic and have been correlated to the degree of cation distortion for the $N(CH_3)_4^+$ cation in a variety of crystal symmetries. In the present study, the overall spectral features of the $N(CH_3)_4^+$ cation are found to be very similar to those reported for $N(CH_3)_4^+$ in dilute aqueous[98,99] and methanol solutions,[98] especially in the methyl deformation and stretching regions where the number, frequencies, and relative intensities of the lines are nearly identical. It can therefore be concluded that in $N(CH_3)_4^+M(OTeF_5)_6^-$ salts the distortion of the $N(CH_3)_4^+$ cations from tetrahedral symmetry must also be minimal. Moreover, it has been shown that a correlation exists between the degree of cation dissociation and the positions of the CH stretching bands, $\nu_5(E)$ and $\nu_{14}(T_2)$, which are presumed to overlap and which vary in frequency from 3008

cm^{-1} for the most distorted $N(CH_3)_4^+$ cation in $N(CH_3)_4^+I^-$ to the least distorted cases $N(CH_3)_4^+ClO_4^-$ (3042 cm^{-1}) and 5 M $N(CH_3)_4^+Cl^-$ in D_2O (3036 cm^{-1}).[98,99] The high-frequency positions of these lines in all three $N(CH_3)_4^+M(OTeF_5)_6^-$ salts in the present study (3050–3052 cm^{-1}) are also consistent with $N(CH_3)_4^+$ cations that are little distorted from T_d symmetry. This band, however, broadens somewhat in going from $As(OTeF_5)_6^-$ to $Sb(OTeF_5)_6^-/Bi(OTeF_5)_6^-$ and the broadening may arise from removal of the proposed accidental coincidence of $\nu_5(E)$ and $\nu_{14}(T_2)$ and/or removal of their degeneracies by symmetry lowering at the CH_3 sites. Previous studies have shown that this band is split in salts when the site symmetry is lowered sufficiently.[99] However, examination of the crystal structures of $N(CH_3)_4^+M(OTeF_5)_6^-$ shows that the nitrogen atom of $N(CH_3)_4^+$ possesses the highest site symmetry, C_i, in $N(CH_3)_4^+Bi(OTeF_5)_6^-$ whereas the $N(CH_3)_4^+$ cations of the arsenic and antimony anions both possess site symmetries of C_1. The broadening of the $\nu_5(E)/\nu_{14}(T_2)$ band in the case of the bismuth salt is therefore likely to be associated with the short C···F contacts and hydrogen bonding interactions with the fluorines of $N(CH_3)_4^+Bi(OTeF_5)_6^-$ noted earlier (see X-ray crystallography section) which lower the site symmetry of the CH_3 groups.

There are several weak to moderate intensity bands at 800–910 cm^{-1} in these spectra which do not appear in any of the Raman spectra of known salts containing the $N(CH_3)_4^+$ cation nor do they appear in the Raman spectra of other $OTeF_5$ derivatives. Similar bands are also observed in the Raman spectrum of $N(CH_2CH_3)_4^+Sb(OTeF_5)_6^-$. Although these bands are likely to be associated with the anion, for the present, they cannot be assigned with any degree of confidence. One possible explanation is that they arise from binary and combination bands which are normally expected to be weak in the Raman spectrum. The observed bands could, however, arise from the intense A_1 modes of the anion by Fermi resonance of combination A_1 modes ($\nu_i(A_1) + \nu_j(A_1)$) or first overtone A_1 ($2\nu_i(A_1)$) modes of the anion with intense fundamental A_1 modes ($\nu_k(A_1)$) so that the normally weak combination/binary modes borrow most of their intensity from the A_1 fundamentals.

Conclusions

Synthetic approaches have been devised which lead to the preparation of pure tetraalkylammonium salts of $M(OTeF_5)_6^-$ (M = As, Sb, Bi) anions.

Multi-NMR spectroscopy has been used to define the series of pnicogen anions in solution, and the observation of all three quadrupolar nuclei and their spin–spin couplings with tellurium in the Lewis base solvent, CH_3CN, affirms their non-lability on the NMR time scale and affords insight into the nature of the spin–spin coupling contribution in the homologous series.

X-ray crystallographic studies indicate that access to free valence electron pairs on the oxygen atoms of the arsenic and antimony anions appears to be comparable or less than that of the divalent $Ti(OTeF_5)_6^{2-}$ anion. However, the pnicogen anion series, by virtue of its single negative charge and anticipated strong Lewis acid characters of the $M(OTeF_5)_5$ precursors, is anticipated to be less basic than the previously studied $B(OTeF_5)_4^-$, $Pd(OTeF_5)_4^{2-}$, $Ti(OTeF_5)_6^{2-}$, and $Nb(OTeF_5)_6^-$ anions and should therefore be among the best candidates for least-coordinating anions among the $OTeF_5$ derivatives.

Experimental Section

Materials and Apparatus. Manipulations involving volatile materials were performed under strictly anhydrous conditions on a Pyrex glass vacuum line equipped with greaseless J. Young PTFE stopcocks. Nonvolatile materials were handled in the dry nitrogen atmosphere of a glovebox (Vacuum Atmospheres Model DLX).

The reagents $HOTeF_5$,[102] $B(OTeF_5)_3$,[25] $Sb(OTeF_5)_3$,[34] and $As(OTeF_5)_5$[32] were prepared as described previously. Literature methods were used for the purification of $N(CH_2CH_3)_4^+Cl^-$ (Fluka),[103] $N(CH_3)_4^+Cl^-$ (Fluka),[103] BiF_5 (Ozark-Mahoning),[8] SO_2ClF (Aldrich),[104] and CH_3CN (Caledon HPLC Grade).[105]

The literature preparation of $Xe(OTeF_5)_2$ from XeF_2 requires the use of a large excess of $HOTeF_5$.[106] In preference to this, the following synthesis has been employed in the present work. Boron tris[pentafluorooxotellurate(VI)] (10.6631 g, 14.68 mmol) was loaded into a dry 0.5-in FEP tube in the drybox. The tube was then placed into a cold-well, located inside the drybox, and cooled to −196 °C. Xenon difluoride (3.7482 g, 22.14 mmol) was added on top of the cold $B(OTeF_5)_3$. The FEP tube was kept cold and fitted with a Kel-F valve before removal from the drybox. The cold tube was attached to a glass vacuum line and Freon 114 (ca. 6 cm depth) distilled on to the solid reagents at −196 °C. The tube was placed in a −78 °C cold bath, attached to a metal vacuum line, and the open tube and vacuum manifold were pressurized to 1 atm with dry N_2. The reaction mixture was further warmed to −8 °C over a period of 1 h. During this time, BF_3 slowly evolved and was periodically pumped away in order to maintain the pressure in the manifold and reaction tube at ca. 1 atm. As the reaction rate slowed, the tube was agitated and allowed to warm to room temperature in order to complete the reaction. When no further pressure increase was noted the solvent was slowly pumped away, leaving a very pale yellow microcrystalline powder in essentially quantitative yield (13.2162 g, 98%). The tube was pressurized with dry N_2 and stored at −78 °C until required.

Dichloromethane (Caledon) was refluxed over CaH_2 for 1 h, distilled on to Type 4A molecular sieves, and, after standing over the sieves for 24 h, distilled *in vacuo* into a dry Pyrex storage vessel prior to use. Ethyl acetate (Fisher) was refluxed over P_4O_{10} for 1 h, distilled on to Type 4A molecular sieves, and, after standing over the sieves for 24 h, distilled *in vacuo* on to fresh Type 4A molecular sieves for storage. Freon 114 ($CClF_2$-$CClF_2$; Aldrich) was stored over P_4O_{10} and distilled *in vacuo* into a dry Pyrex storage vessel prior to use.

$N(CH_3)_4^+OTeF_5^-$. Pentafluorooxotelluric acid (7.7413 g, 32.309 mmol) was distilled *in vacuo* into one bulb of a two-bulb reaction vessel equipped with a glass sinter and J. Young stopcock separating the two bulbs. The vessel was taken into the drybox and anhydrous $N(CH_3)_4^+Cl^-$ (3.5454 g, 32.349 mmol) loaded into the other bulb. The vessel was re-attached to the glass vacuum line and anhydrous acetonitrile (*ca.* 30 mL) distilled on to the $N(CH_3)_4^+Cl^-$ at −196 °C. The stopcock separating the two bulbs was opened and the $HOTeF_5$ distilled on top of the CH_3CN. The reaction mixture was slowly warmed, with stirring, to 0 °C at which point reaction began to take place. The mixture was warmed to room temperature and the reaction was deemed to be complete when all the $N(CH_3)_4^+Cl^-$ had dissolved. The solution was filtered through the glass sinter to give a clear, pale yellow solution. The CH_3CN and liberated HCl were pumped off leaving a pale yellow solid. This crude material was recrystallized from CH_3CN to give a very pale yellow crystalline solid (9.9346 g, 98.3%).

$N(CH_2CH_3)_4^+OTeF_5^-$. Tetraethylammonium pentafluorooxotellurate(VI) was prepared in a similar fashion to $N(CH_3)_4^+OTeF_5^-$ (*vide supra* $N(n\text{-}CH_3CH_2CH_2CH_2)_4^+OTeF_5^-$)[28,107] using the following quantities of reagents: $HOTeF_5$ (6.7491 g, 28.168 mmol); $N(CH_2CH_3)_4^+Cl^-$ (4.6863 g, 28.281 mmol). Dichloromethane (*ca.* 20 mL) was used as the reaction solvent instead of CH_3CN. The crude product was recrystallized twice from ethyl acetate to yield a slightly off-white crystalline solid (8.5664 g, 83%).

$Bi(OTeF_5)_5$. The preparation was carried out in a two-limb Pyrex vessel, each limb of which was fitted with a J. Young stopcock. The two limbs were connected together via another J. Young stopcock. The BiF_5 (0.2911 g, 0.9577 mmol) and $B(OTeF_5)_3$ (1.3638 g, 1.8769 mmol) were loaded into separate limbs of the reaction vessel in the drybox. The vessel was attached to a glass vacuum line and evacuated and dry Freon-114 distilled into the limb containing the $B(OTeF_5)_3$ at −196 °C. The limb was allowed to warm to room temperature in order to effect dissolution of the $B(OTeF_5)_3$ in the Freon 114. The limb containing the BiF_5 was cooled to −78 °C and the interconnecting stopcock opened so that the $B(OTeF_5)_3$/Freon 114 solution could be transferred on to the BiF_5. The reaction mixture was warmed to −10 °C at which point slow reaction began to take place. On warming, with stirring, to 0 °C the reaction

(102) Sladky, F. *Inorganic Syntheses*; Shreeve, J. M., Ed., Wiley-Interscience: New York, 1986; Vol. 24, p 34.
(103) Dillon, K. B.; Platt, A. W. G. *J. Chem. Soc., Dalton Trans.* **1982**, 1199.
(104) Schrobilgen, G. J.; Holloway, J. H.; Granger, P.; Brevard, C. *Inorg. Chem.* **1978**, *17*, 980.
(105) Winfield, J. M. *J. Fluorine Chem.* **1984**, *25*, 91.
(106) Sladky, F. *Inorganic Syntheses*; Shreeve, J. M., Ed., Wiley-Interscience: New York, 1986; Vol. 24, p 36.
(107) Strauss, S. H.; Abney, K. D.; Anderson, O. P. *Inorg. Chem.* **1986**, *25*, 2805.

mixture became bright yellow and steady evolution of BF_3 was observed. After 1 h BF_3 evolution had ceased; the reaction mixture was cooled to −78 °C and the BF_3 pumped off. The mixture was allowed to warm to room temperature for 30 min. The pale yellow supernatant liquid was decanted off into the other limb leaving the $Bi(OTeF_5)_5$ as a fine yellow powder (0.9661 g, 72%).

$N(CH_3)_4^+Bi(OTeF_5)_6^-$ (1), $N(CH_3)_4^+As(OTeF_5)_6^-$ (2), $N(CH_2CH_3)_4^+Sb(OTeF_5)_6^-$ (3), and $N(CH_3)_4^+Sb(OTeF_5)_6^-$ (4) and Crystal Growing. (a) Compound 1. In the drybox, $Bi(OTeF_5)_5$ (0.4776 g, 0.3407 mmol) and $N(CH_3)_4^+OTeF_5^-$ (0.1078 g, 0.3447 mmol) were loaded into separate limbs of a two-limb vessel equipped with J. Young stopcocks. The vessel was attached to a glass vacuum line and SO_2ClF solvent (ca. 5 mL) distilled *in vacuo* on to the $Bi(OTeF_5)_5$ at −78 °C. The mixture was allowed to warm to 0 °C and the resulting solution poured on to the $N(CH_3)_4^+OTeF_5^-$ in the other limb. The reaction mixture was left stirring at room temperature overnight. A very pale yellow solution containing a small amount of white insoluble material resulted. The solution was warmed to 35 °C; however the white material remained insoluble. The pale yellow supernatant solution was decanted into the other limb of the vessel. An equal volume of Freon-114 was distilled into the limb containing the white solid. The Freon 114 vapor was allowed to diffuse into the SO_2ClF solution over a period of 48 h. This resulted in the formation of clusters of large, pale yellow crystals or prisms of $N(CH_3)_4^+Bi(OTeF_5)_6^-$ (0.3283 g, 53.8%). After decantation of the supernatant and vacuum drying of the crystals, the vessel was then transferred to a drybox equipped with a microscope and cut open. The crystals were sealed in 0.3–0.4 mm Lindemann glass capillaries and stored at room temperature prior to mounting on the diffractometer. A preliminary observation of the sealed crystals under a polarizing microscope revealed that most of them were single crystals. The crystal used in this study was a prism with dimensions 0.3 × 0.45 × 0.5 mm.

(b) Compound 2. The $As(OTeF_5)_5$ (0.9050 g, 0.7138 mmol) and $N(CH_3)_4^+OTeF_5^-$ (0.2238 g, 0.7158 mmol) were loaded into separate limbs of a two-limb Pyrex vessel equipped with J. Young stopcocks in the drybox. The vessel was attached to a glass vacuum line and SO_2ClF (ca. 4 mL) distilled on to the $As(OTeF_5)_5$ at −78 °C. On warming to room temperature, the $As(OTeF_5)_5$ dissolved in the SO_2ClF and the resulting solution was then poured on to the $N(CH_3)_4^+OTeF_5^-$. The other limb was rinsed three times with SO_2ClF in order to ensure that all the $As(OTeF_5)_5$ had transferred. The $N(CH_3)_4^+OTeF_5^-$ rapidly dissolved giving a clear colorless solution. Freon 114 was distilled *in vacuo* into the empty limb of the vessel while the stopcock between the two limbs was kept closed. When the Freon 114 had warmed to room temperature, the interconnecting stopcock was opened, allowing the Freon 114 vapor to diffuse into the SO_2ClF solution. Clusters of large colorless plate-like crystals as well as isolated cubic prisms formed over a period of 24 h. The supernatant liquid comprised two layers which were decanted away from the crystals. The latter were rinsed with Freon 114 and pumped dry in dynamic vacuum (0.6760 g, 60%) before being transferred in a drybox. Some of the crystals were cut with a scalpel and mounted in 0.3, 0.4, and 0.5 mm Lindemann glass capillaries and stored at room temperature prior to mounting on the diffractometer since they proved to undergo a phase transition when kept at −65 °C. The crystal used in this study was a thick plate with dimensions 0.2 × 0.5 × 0.55 mm.

(c) Compound 3. Freshly sublimed $Sb(OTeF_5)_3$ (2.0974 g, 2.5043 mmol) was loaded into one limb of a two-limbed vessel equipped with J. Young stopcocks. The $N(CH_2CH_3)_4^+OTeF_5^-$ (0.9314 g, 2.5252 mmol) was added on top of the $Sb(OTeF_5)_3$. $Xe(OTeF_5)_2$ (1.5553 g, 2.5561 mmol) was added into the empty limb of the vessel. The vessel was then removed from the drybox and attached to a glass vacuum line. Sulfuryl chloride fluoride (ca. 5 mL) was distilled *in vacuo* on to the $Sb(OTeF_5)_3$/$N(CH_2CH_3)_4^+OTeF_5^-$ mixture at −78 °C. The solids dissolved on warming to room temperature giving a clear colorless solution of $N(CH_2CH_3)_4^+Sb(OTeF_5)_4^-$. The SO_2ClF was distilled off the $N(CH_2CH_3)_4^+Sb(OTeF_5)_4^-$ and condensed on to the $Xe(OTeF_5)_2$ at −78 °C. The $Xe(OTeF_5)_2$ dissolved in the SO_2ClF; this solution was poured through the side arm on to the $N(CH_2CH_3)_4^+Sb(OTeF_5)_4^-$ held at −78 °C. On warming the mixture to 0 °C, evolution of Xe gas was observed and a clear colorless solution resulted. The solution was allowed to warm to room temperature and the SO_2ClF slowly distilled off until a significant quantity of crystals had formed and did not redissolve on agitating the mixture. The solution was warmed in order to redissolve the crystalline material and then allowed to stand at room temperature for 48 h. A crop of hexagonal plates was obtained, but they proved to be unsuitable for an X-ray crystallography study. Consequently, the mother liquor was decanted off and the crystals were redissolved in a small quantity of fresh SO_2ClF (ca. 1 mL). Freon 114 (ca. 1 mL) was carefully distilled on top of the SO_2ClF solution at 0 °C. The two-phase system was allowed to stand at room temperature for 48 h resulting in the formation of large, colorless plate-like crystals of $N(CH_2CH_3)_4^+Sb(OTeF_5)_6^-$, some of them presenting triangular edges. The solvents were drained away from the crystals which was then pumped dry in dynamic vacuum. The crystals were finally rinsed with a small amount of Freon 114 and dried in dynamic vacuum before being transferred in a drybox where they were mounted and sealed in 0.4–0.5 mm Lindemann glass capillaries. The crystals were kept at room temperature prior to mounting on the diffractometer since they appeared to undergo a phase transition when kept in solid dry ice. The crystals, observed under a polarizing microscope, appeared to be single or perfectly twined. The crystal used in this study was triangular with dimensions 1.2 × 0.9 × 0.45 mm.

(d) Compound 4. The $N(CH_3)_4^+Sb(OTeF_5)_6^-$ salt was prepared in a similar fashion to $N(CH_2CH_3)_4^+Sb(OTeF_5)_6^-$ using the following quantities of reagents: $Sb(OTeF_5)_3$ (1.2240 g, 1.461 mmol), $N(CH_3)_4^+OTeF_5^-$ (0.4588 g, 1.467 mmol), and $Xe(OTeF_5)_2$ (0.9556 g, 1.5705 mmol). After completion of the reaction, all volatile materials were pumped off leaving a sticky solid mass. This was redissolved in fresh SO_2ClF (ca. 3.5 mL) and an equal volume of Freon 114 allowed to diffuse into the solution at room temperature. Over a period of 5 days, two distinct liquid layers formed and a cluster of poorly formed crystals deposited. The liquid layers were poured off the crystals and the solvents pumped off. The crystalline material was redissolved in fresh SO_2ClF (3.5 mL). Freon 114 (5 mL) was allowed to diffuse into the SO_2ClF solution at room temperature. Large, colorless crystals of $N(CH_3)_4^+Sb(OTeF_5)_6^-$ grew overnight. The supernatant solution was poured off; the crystals were allowed to drain and then pumped in dynamic vacuum (0.6739 g, 28%) before being transferred in a drybox where they were mounted and sealed in 0.3, 0.4, and 0.5-mm Lindemann glass capillaries. The crystals were kept at room temperature prior to mounting on the diffractometer. The crystal used in this study was a prism with dimensions 0.35 × 0.5 × 0.6 mm.

Following data collection, the Raman spectra of the single crystals were recorded and shown to be identical with those of the bulk samples.

Nuclear Magnetic Resonance Spectroscopy. The NMR spectra were recorded unlocked (field drift <0.1 Hz h^{-1}) on a Bruker AM-500 spectrometer equipped with an 11.744 T cryomagnet. The ^{19}F spectra were obtained using a 5-mm combination $^1H/^{19}F$ probe operating at 470.599 MHz. The spectra were recorded in a 32 K memory. A spectral width setting of 20 kHz was employed, yielding a data point resolution of 1.221 Hz/data point and an acquisition time of 0.82 s. No relaxation delays were applied. Typically, 5000–11000 transients were accumulated. The pulse width corresponding to a bulk magnetization tip angle, θ, of approximately 90° was equal to 1 μs. No line-broadening parameters were used in the exponential multiplication of the free induction decays prior to Fourier transformations.

The ^{75}As, ^{121}Sb, ^{123}Sb, ^{125}Te, and ^{209}Bi NMR spectra were obtained by using a broad-band VSP probe tunable over the range 23–202 MHz. The observing frequencies were the following: ^{75}As (85.637 MHz), ^{121}Sb (119.696 MHz), ^{123}Sb (64.819 MHz), ^{125}Te (157.791 MHz), and ^{209}Bi (80.381 MHz). The ^{75}As, ^{121}Sb, ^{123}Sb, and ^{209}Bi spectra were recorded in an 8K memory. The spectral width setting was 20 kHz, which yielded a data point resolution of 4.9 Hz/data point and an acquisition time of 0.205 s. The ^{125}Te spectra were recorded in a 16 K memory with a spectral width of 50 kHz, yielding a data point resolution of 6.1 Hz per data point and an acquisition time of 0.164 s. No relaxation delays were applied. The number of transients that were accumulated varied with the nuclide under observation with typical values being 14000 (^{75}As), 7000 (^{121}Sb), 36000 (^{123}Sb), 200000–400000 (^{125}Te), and 5500 (^{209}Bi). The pulse widths corresponding to a bulk magnetization tip angle, θ, of approximately 90° were ^{75}As (15.0 μs), ^{121}Sb (13.0 μs), ^{123}Sb (15.8 μs), ^{125}Te (18.0 μs), and ^{209}Bi (14.0 μs). A line broadening parameter of 1.5 Hz was applied in the exponential multiplication of the free induction decay prior to Fourier transformation.

Spin–lattice relaxation times, T_1, were determined for degassed, vacuum-sealed samples by the standard $(\pi-\tau-\pi/2)$ sequence with accumulation of the free induction decay after the $\pi/2$ pulse.

The spectra were referenced externally at ambient temperature to the respective standard samples: neat $CFCl_3$ (^{19}F), neat $(CH_3)_2Te$ (^{125}Te), 0.1 M $N(C_2H_5)_4^+AsF_6^-$ in CH_3CN (^{75}As), 0.1 M $N(C_2H_5)_4^+SbF_6^-$ in CH_3CN ($^{121,123}Sb$), and a saturated solution of $N(CH_3)_4^+BiF_6^-$ in CH_3CN (^{209}Bi). The chemical shift convention used is that a positive sign signifies a chemical shift to high frequency of the reference compound.

The ^{19}F NMR samples were prepared in 4-mm o.d. FEP or 5-mm medium-wall glass NMR tubes, whereas samples for ^{75}As, ^{121}Sb, ^{123}Sb, ^{125}Te, and ^{209}Bi NMR spectroscopy were prepared in 9-mm o.d. FEP

NMR tubes as described previously.[108] Solids were weighed into the FEP tubes in the drybox. The tube was closed with a Kel-F valve and transferred to a glass vacuum line where CH_3CN solvent was distilled *in vacuo* on to the solid at −78 °C. The tubes were heat-sealed in dynamic vacuum while keeping the contents frozen to −196 °C. The sealed FEP sample tubes were inserted into 10- or 5-mm thin-walled precision NMR tubes (Wilmad) before being placed in the probe.

Crystal Structure Determination of $N(CH_3)_4^+Bi(OTeF_5)_6^-$ (1), $N(CH_3)_4^+As(OTeF_5)_6^-$ (2), $N(CH_2CH_3)_4^+Sb(OTeF_5)_6^-$ (3), and $N(CH_3)_4^+)Sb(OTeF_5)_6^-$ (4). (a) Collection and Reduction of X-ray Data. The crystals of compounds **1**, **2**, and **3** were centered on a Siemens/Syntex $P2_1$ diffractometer, using silver radiation monochromatized with a graphite crystal ($\lambda = 0.56086$ Å). A crystal of compound **4** was centered on a Siemens P4 diffractometer equipped with a rotating anode, using molybdenum radiation monochromatized with a graphite crystal ($\lambda = 0.71073$ Å). The data sets of compounds **2**, **3**, and **4** were collected at ambient temperature. Attempts to collect data sets at −66 °C resulted in phase transitions and powdering of crystals. During data collection the intensities of three standard reflections were monitored every 97 reflections to check for crystal stability and alignment.

The experimental values for the antimony compound (**3**), when they differ from those of the bismuth compound (**1**), are given in square brackets. Accurate cell dimensions were determined at −62 °C [24 °C] from a least-squares refinement of the setting angles (χ, ϕ, and 2θ) obtained from 25 [18] accurately centered reflections (with 21.09° [12.44°] $\leq 2\theta \leq$ 35.23° [29.06°]) chosen from a variety of points in reciprocal space. The examination of the peak profiles revealed single peaks. Integrated diffraction intensities were collected using a θ–2θ scan technique with scan rates varying from 1.5 to 14.65 deg/min (in 2θ) so that the weaker reflections were examined most slowly to minimize counting errors. The data were collected with 0 [0] $\leq h \leq$ 12 [11], −12 [0] $\leq k \leq$ 12 [19], and −13 [−21] $\leq l \leq$ 13 [21] and with 3° [3°] $\leq 2\theta \leq$ 45° [35°]. For compound **1**, the intensities of the standards changed regularly to about 89% of their original values during the course of the data collection; this decomposition was later corrected by scaling the data linearly between each set of standards. Only a 4.7% decay was observed for compound **3**. A total of 4499 [5556][109] reflections were collected out of which 144 [180] were standard reflections. After averaging of equivalent reflections, 4238 [2536] unique reflections remained. A total of 3734 [1743] reflections, satisfying the condition $I \geq 2\sigma(I)$, were used for structure solution.

For the arsenic compound (**2**), accurate cell dimensions were determined at 24 °C from a least-squares refinement of the setting angles (χ, ϕ, and 2θ) obtained from 22 accurately centered reflections (with 14.54° $\leq 2\theta \leq$ 29.36°) chosen from a variety of points in reciprocal space. Integrated diffraction intensities were collected using an ω scan technique with scan rates varying from 1.5 to 14.65 deg/min (in 2θ). Data were collected in three steps, and only the reflections ($-h + k + l = 3n$) were collected since the system was known to be rhombohedral R. In the first step, the data were collected with $0 \leq h \leq 12$, $0 \leq k \leq 12$, and $0 \leq l \leq 67$ and with 3° $\leq 2\theta \leq$ 45°. When the system was confirmed to be trigonal, second and third sets (in brackets) of data were collected with 0 [0] $\leq h \leq$ 12 [12], −12 [−12] $\leq k \leq$ 12 [0], and −67 [0] $\leq l \leq$ 0 [67]. A decay of 7% was observed for compound **2**. A total of 6924 reflections were collected out of which 225 were standard reflections. After averaging of equivalent reflections, 2107 unique reflections remained. A total of 1375 reflections, satisfying the condtion $I \geq 2\sigma(I)$, were used for structure solution.

Accurate cell dimensions were determined for the antimony compound (**4**) at 24 °C from a least-squares refinement of the setting angles (χ, ϕ, and 2θ) obtained from 41 accurately centered reflections (with 9.43° $\leq 2\theta \leq$ 24.98°) chosen from a variety of points in reciprocal space. Integrated diffraction intensities were collected using a θ–2θ scan technique with scan rates varying from 1.5 to 14.65 deg/min (in 2θ). The data were collected with $-1 \leq h \leq 25$, $-1 \leq k \leq 14$, and $-27 \leq l \leq 26$ and with 2° $\leq 2\theta \leq$ 60°. A decay of 6% was observed. A total of 6166 reflections were collected out of which 450 were standard reflections. A total of 4910 unique reflections remained after averaging of equivalent reflections. A total of 2001 reflections, satisfying the condition $I \geq 2\sigma(I)$ were used for structure solution.

For all four compounds, corrections were made for Lorentz and polarization effects. Absorption corrections were applied to the data of compounds **1** and **2** by using the program DIFABS,[110] while for compound **4** the ϕ-scan method ($\Delta\phi = 10°$, $\mu\bar{R} = 1.443$) was used. No absorption corrections were applied for compound **3**.

(b) Crystal Data. Compound **1** ($f_w = 1714.73$): crystallizes in the triclinic system, space group $P\bar{1}$; $a = 8.945(2)$ Å, $b = 9.217(2)$ Å, $c = 10.029(2)$ Å, $\alpha = 100.03(3)°$, $\beta = 99.95(3)°$, $\gamma = 98.06(3)°$; $V = 789.5$ Å^3; $D_{calc} = 3.606$ g cm^{-3} for $Z = 1$. Ag(Kα) radiation ($\lambda = 0.56086$ Å, μ(AgKα) = 60.4 cm^{-1}) was used. Compound **2** ($f_w = 1580.67$): crystallizes in the trigonal system, space group $R\bar{3}$; $a = 10.109(2)$ Å, $c = 55.443(18)$ Å; $V = 4907.0$ Å^3; $D_{calc} = 3.209$ g cm^{-3} for $Z = 6$. Ag(Kα) radiation ($\lambda = 0.56086$ Å, μ(AgKα) = 34.2 cm^{-1}) was used. Compound **3** ($f_w = 1683.6$): crystallizes in the monoclinic system, space group $C2/c$; $a = 10.506(3)$ Å, $b = 18.370(6)$ Å, $c = 20.352(7)$ Å, $\beta = 91.23(2)°$; $V = 3926.9$ Å^3; $D_{calc} = 2.848$ g cm^{-3} for $Z = 4$. Ag(Kα) radiation ($\lambda = 0.56086$ Å, μ(AgKα) = 27.7 cm^{-1}) was used. Compound **4** ($f_w = 1627.5$): crystallizes in the monoclinic system, space group $C2/c$; $a = 17.875(3)$ Å, $b = 10.448(2)$ Å, $c = 19.752(2)$ Å, $\beta = 110.83(1)°$; $V = 3447.8$ Å^3; $D_{calc} = 3.135$ g cm^{-3} for $Z = 4$. Mo(Kα) radiation ($\lambda = 0.71073$ Å, μ(MoKα) = 59.6 cm^{-1}) was used.

(c) Solution and Refinement of the Structures. The program XPREP[111] was used for determining the correct cells and space groups.

Compound 1: The lattice was triclinic primitive ($R_{int} = 0.018$). The structure was shown to be centrosymmetric by an examination of the *E*-statistics (calc, 0.875; theor, 0.968), and consequently the structure was solved in the space group $P\bar{1}$. A first solution was obtained without absorption corrections by direct methods which located the positions of the bismuth and tellurium atoms on special ($d\bar{1}$) and general positions, respectively. The full-matrix least-squares refinement of the bismuth and tellurium atom positions and isotropic thermal parameters gave a conventional agreement index R ($=\Sigma||F_o| - |F_c||/\Sigma|F_o|$) of 0.165. A difference Fourier synthesis revealed the remaining oxygen and fluorine atoms of the anion (both on general positions), as well as the nitrogen and carbon atoms of the cation on special ($g\bar{1}$) and general positions, respectively. The presence of the carbon atoms on general positions implied a positional disorder of the cation and consequently the site occupancy factors (s.o.f.) of the carbon atoms were set equal to 0.5 instead of 1.00. Refinement of positional and isotropic temperature parameters for all atoms converged at $R = 0.109$. A significant improvement of the structure was achieved by introducing anisotropic positions for the hydrogen atoms (d(C–H) = 0.96 Å, U(H) fixed to 0.08, s.o.f. fixed to 0.5), reducing R to 0.046. The structure was solved a second time using data that had been corrected empirically for absorption. The initial model used the atomic coordinates and isotropic thermal parameters defined previously for the Bi, Te, O, F, N, C, and H atoms. The solution obtained (R = 0.094) indicated a small improvement over that obtained without absorption corrections ($R = 0.109$). The final refinement was obtained by introducing a weight factor ($w = 1/\sigma^2(F) + 0.002266\sigma F^2$) and an isotropic correction for secondary extinction and gave rise to a residual, R, of 0.0456 ($R_w = 0.0516$). In the final difference map, the maximum and minimum electron densities were 3.52 and −2.22 eÅ^{-3}.

Compound 2. The lattice was trigonal ($R_{int} = 0.059$). The two space groups, which were consistent with the systematic absences, were the centrosymmetric $R\bar{3}$ and the chiral $R3$ space groups. The structure was shown to be centrosymmetric by an examination of the *E*-statistics (calc, 0.993; theor, 0.968), and consequently the structure was solved in the space group $R\bar{3}$. A first solution was obtained without absorption corrections and it was achieved by using the Patterson function which located the arsenic and nitrogen atoms on special positions (a$\bar{3}$, As(1); b$\bar{3}$, As(2); and c3, N(1), respectively) and the tellurium atoms on general positions. The full-matrix least-squares refinement of the arsenic, tellurium, and nitrogen atom positions and isotropic thermal parameters gave a conventional agreement index R of 0.228. Successive difference Fourier syntheses revealed the positions of one carbon atom and all the remaining oxygen and fluorine atoms on general positions as well as that of the other carbon atom on the special position c3. Refinement of positional and isotropic temperature parameters for all atoms (the calculated positions for the hydrogen atoms with d(C–H) = 0.96 Å, U(H) fixed to 0.08, were also introduced) converged at $R = 0.135$ and revealed somewhat large thermal parameters for the oxygen and fluorine atoms associated with one of the anions (Table 6). The structure was considerably improved by introducing anisotropic thermal parameters for the As, Te, O, and N atoms, giving a residual R of 0.0768. At that point, the considerable difference in the values of the thermal parameters of O1 and O2 [U(O1) = 0.239 Å^2 and U(O2) = 0.053 Å^2], as well as of the As–O–Te angles [152(2) and 139.9(9)°, respectively], suggested

(108) Christe, K. O.; Curtis, E. C.; Dixon, D. A.; Mercier, H. P.; Sanders, J. C. P.; Schrobilgen, G. J. *J. Am. Chem. Soc.* **1991**, *113*, 3351.

(109) For compound **3**, the strongest reflections at very low angles could not be recorded under normal conditions of data acquisition, i.e. maximum intensity, 1.5 kW Ag X-rays without attenuation; the power had to be decreased to 900 kW, and another set of data was collected with $0 \leq h \leq 0$, $0 \leq k \leq 7$, and $-7 \leq l \leq 4$.

(110) Walker, N.; Stuart, D. *Acta Crystallogr.* **1983**, *A39*, 158.

a possible disorder for the O(1) atom: the ellipsoid associated with O(1) was exhibiting a very strong anisotropy perpendicular to the As(1)---Te(1) direction. Because of the disorder, the choice of the space group was double checked by carefully re-examining the symmetry equivalents and systematic absences. The structure was solved another time, excluding both oxygen atoms. Interestingly, the resulting Fourier difference revealed only one atom bonded to As(2), but two atoms to As(1). As expected, the introduction of the two partial positions for the O(1) atom (s.o.f. O(1A) = 0.64; s.o.f. O(1B) = 0.36) was accompanied by a decrease in the values of the thermal parameters and, more importantly, by better agreement of the As–O and Te–O bond lengths and As–O–Te angles in the two anions. The structure was solved a second time using data that had been corrected empirically for absorption. The initial model used the atomic coordinates and isotropic thermal parameters defined previously for the Sb, Te, O, F, N, C, and H atoms. In the final refinement, O(1A) and O(1B) were kept isotropic because of the presence of the positional disorder; the weight factor was set equal to zero and it gave rise to a residual, R, of 0.0644 (R_w = 0.0540). In the final difference map, the maximum and the minimum electron densities were 1.36 and –1.22 eÅ^{-3}.

Compound 3: The lattice was monoclinic C (R_{int} = 0.022). Two space groups were consistent with the systematic absences, the centrosymmetric $C2/c$ and the non-centrosymmetric Cc space groups. The structure was shown to be centrosymmetric by an examination of the E-statistics (calc, 0.907; theor, 0.968) and was solved in the space group $C2/c$. A first solution was obtained without absorption corrections and was achieved by direct methods which located the positions of the antimony and tellurium atoms on special ($a\bar{1}$) and general positions, respectively. The full-matrix least-squares refinement of the antimony and tellurium atom positions and isotropic thermal parameters gave a conventional agreement index R of 0.215. Successive difference Fourier syntheses revealed the positions of all the remaining oxygen, fluorine, and carbon atoms on general positions as well as that of the nitrogen atom on the special position e2. Refinement of positional and isotropic temperature parameters for all atoms converged at R = 0.162. Introduction of anisotropic thermal parameters for all the atoms markedly improved the crystallographic residual, since the anisotropies of all the light atoms and tellurium atoms were very large (Table 25), reducing R to 0.0528 (the calculated positions for the hydrogen atoms [d(C–H) = 0.96 Å, U(H) fixed to 0.10] were also included). The anisotropies of the carbon atoms were also high. The final refinement was obtained by setting the weight factor equal to zero and gave rise to a residual, R, of 0.0548 (R_w = 0.0461). In the final difference map, the maximum and the minimum electron densities were 0.81 and –0.53 eÅ^{-3}. An empirical absorption correction was applied, but no significant improvement in the refinement was observed.

Compound 4: The lattice was monoclinic C (R_{int} = 0.028). The structure was solved in the space group $C2/c$ and in a way very similar to that used for compound **3**. The full-matrix least-squares refinement of positional and isotropic temperature parameters for all atoms (the calculated positions for the hydrogen atoms included) converged at R = 0.184, without absorption corrections. In general, the anisotropies of all the light atoms and tellurium atoms were much smaller than those observed for compound **3**. Nevertheless, the introduction of anisotropic thermal parameters for the Sb, Te, O, F, and N atoms significantly improved the structure, reducing R to 0.073. The anisotropies of the carbon atoms were also high. The structure was solved a second time using data that had been corrected empirically for absorption. The final refinement was obtained by setting the weight factor to zero and gave rise to a residual, R, of 0.0710 (R_w = 0.0599). In the final difference map, the maximum and the minimum electron densities were 0.92 and –0.85 eÅ^{-3}.

All calculations were performed on a 486 personal computer using the SHELXTL PLUS (Sheldrick, 1990)[111] determination package for structure solution and refinement as well as structure determination molecular graphics.

Raman Spectroscopy. Raman spectra were recorded on a Jobin-Yvon Mole S-3000 triple spectrograph system equipped with a 0.32-m prefilter, adjustable 25-mm entrance slit, and a 1.00-m monochromator. Holographic gratings were used for the prefilter (600 grooves mm^{-1}, blazed at 500 nm) and monochromator (1800 grooves mm^{-1}, blazed at 550 nm) stages. An Olympus metallurgical microscope (Model BHSM-L-2) was used for focusing the excitation laser to a 1-μm spot on the sample. The 514.5-nm line of a Spectra Physics Model 2016 Ar ion laser was used for excitation of the sample. Spectra were recorded at ambient temperature on powdered microcrystalline samples sealed in baked-out Pyrex melting point capillaries and on the single crystal used for X-ray determination sealed in its original Lindemann capillary. The powdered material was obtained by carefully grinding five or six large crystals inside the drybox using an agate mortar and pestal.

The spectra were recorded by signal averaging using a Spectraview-2D CCD detector equipped with a 25-mm chip (1152 × 298 pixels) and at a laser power of 20 mW at the sample and slit settings corresponding to a resolution of 1 cm^{-1}. A total of 10 reads having 30-s integration times were summed. Spectral line positions are estimated to be accurate to ±1 cm^{-1}.

Acknowledgment. We thank the donors of the Petroleum Research Fund, administered by the American Chemical Society, for support of this work under ACS-PRF No. 26192-AC3. We also thank the Natural Sciences and Engineering Research Council of Canada for support in the form of an operating grant and Dr. J. Britten, McMaster X-ray Facility, for his help with the absorption corrections.

Supplementary Material Available: A structure determination summary (Tables 9–12), final atomic coordinates and equivalent isotropic thermal parameters (Tables 13–16), anisotropic thermal parameters (Tables 17–20) and hydrogen atomic coordinates (Tables 21–24), a complete list of distances and angles (Table 25), a list of O′–M–O–Te torsion angles (Table 26), stereoview ORTEP drawings of the packing in the unit cells, and a packing diagram of the unit cell of $N(CH_3)_4^+Bi(OTeF_5)_6^-$ showing the shortest C···F contacts (41 pages); tabulations of observed and calculated structure factors (Tables 27–30) (32 pages). This material is contained in many libraries on microfiche, immediately follows this article in the microfilm version of the journal, and can be ordered from the ACS; see any current masthead page for ordering information.

(111) Sheldrick, G. M. (1990); SHELXTL PLUS Release 4.21/V. Siemens Analytical X-Ray Instruments, Inc., Madison, WI.